Ultrasonic investigation of hydrodynamics and mass transfer in a gas-liquid(-liquid) stirred vessel

Cents, A. H. G.; Brilmant, D. W. F.; Versteeg, G. F.

Published in:
International Journal of Chemical Reactor Engineering

DOI:
10.2202/1542-6580.1164

INTERNATIONAL JOURNAL OF CHEMICAL REACTOR ENGINEERING

Volume 3 2005 *Article* A19

Ultrasonic Investigation of Hydrodynamics and Mass Transfer in a Gas-Liquid(-Liquid) Stirred Vessel

A.H.G. Cents* D.W.F. Brilman†

G.F. Versteeg‡

*toine.cents@sasol.com

†d.w.f.brilman@utwente.nl

‡g.f.versteeg@tnw.utwente.nl

ISSN 1542-6580

Ultrasonic Investigation of Hydrodynamics and Mass Transfer in a Gas-Liquid(-Liquid) Stirred Vessel

A.H.G. Cents, D.W.F. Brilman, and G.F. Versteeg

Abstract

The rate of gas-liquid mass transfer is very important in several industrial chemical engineering applications. In many multi-phase reaction systems, however, the mechanism of mass transfer is not well understood. This is for instance the case in Gas-Liquid-Solid (G-L-S) and Gas-Liquid-Liquid (G-L-L) systems. To obtain more knowledge of the mechanism of mass transfer, the mass transfer coefficient, k_L, and the interfacial area, a, should be studied separately. In this work an ultrasonic measurement technique is used to study the local interfacial area in a standard sized vessel, equipped with a Rushton type impeller. This is done in combination with experimental determination of the volumetric mass transfer coefficient, k_La, using the dynamic oxygen method, to obtain values for k_L. The gas hold-up is determined additionally to obtain values for the Sauter mean bubble diameter at different positions in the vessel. In a coalescing air-water system the bubble size was non-uniform throughout the vessel and increased from small bubbles at the impeller along with the flow pattern to larger sizes in the bulk of the vessel. In a non-coalescing electrolyte system the vessel was much more uniform and the bubbles were smaller when compared to the air-water system. To obtain overall values of the mass transfer parameters the local values were integrated according to their volume fraction in the reactor. In both coalescing and non-coalescing systems the overall values for the mass transfer parameters were in good agreement with literature correlations. The addition of small volume-fractions of toluene to an air-water system caused a strong decrease in both the volumetric mass transfer coefficient and in the gas hold-up. The interfacial area increased, however, but it was shown that this was due to the presence of microbubbles in the solution, which do not take part in the mass transfer process. The enhancing effect on gas-liquid mass transfer due to the addition of larger volume-fractions of toluene could be described reasonably well by a homogeneous model of the shuttle mechanism.

KEYWORDS: ultrasound, mass transfer, mapping of stirred vessels, gas-liquid-

liquid, interfacial area, bubble size

1 INTRODUCTION

Many industrial chemical engineering applications are limited by the gas-liquid mass transfer rate. For this reason, accurate knowledge of mass transfer coefficients is necessary to be able to predict the production rates in these processes. In gas-liquid stirred vessels and bubble columns the volumetric mass transfer coefficient, k_La, which is usually sufficient to predict production rates, has been investigated intensively. However, to gain more knowledge about the mechanism of mass transfer, the mass transfer coefficient, k_L, and the gas-liquid interfacial area, a, should be studied separately. This can be established by the use of a chemical method (Danckwerts-plot technique, see Cents et al. (2001)), but this has the disadvantage that this method is confined to some specific chemical systems, which require the addition of electrolytes thereby completely changing the nature of these systems in terms of coalescence and break-up of gas bubbles. Another option is to measure simultaneously the volumetric mass transfer coefficient, k_La, by mass transfer experiments and the gas-liquid interfacial area by using a physical method. Measurement of the interfacial area via physical methods can be performed using photography in combination with determination of the gas hold-up (e.g. Pacek et al. (1994)), using laser scattering (e.g. Calderbank (1958)) or by capillary suction probes (e.g. Barigou and Greaves (1991)). A shared limitation of all these methods is that the interfacial area is determined locally, at a certain, usually fixed, position in the reactor. To obtain a value for the overall interfacial area, values at different positions in the reactor should be integrated according to their volumetric space. When this task is performed, not only an accurate value of the gas-liquid interfacial area is obtained, which can be used together with measurements of k_La to obtain accurate values of the (average) mass transfer coefficient, but also a profile of interfacial areas inside the vessel is obtained. Such a profile contains information about streamlines and coalescence/break-up processes in, for instance, stirred vessels or bubble columns, which can be used to gain understanding about the complex hydrodynamics of these reactors and can be useful in validation of models that are based on Computational Fluid Dynamics (CFD).

Similarly to gas-liquid systems, the rate of mass transfer is usually very important in gas-liquid-liquid systems. As an example, Wachsen et al. (1998) have shown that the biphasic hydroformylation of propylene to butyraldehyde, which is an industrially very important reaction, is (at least partially) mass transfer limited. In this system three gaseous components (propylene, CO and H_2) all react in an aqueous phase containing a homogeneous rhodium catalyst, while the products, (n-and iso-butyraldehyde), form an additional third phase. The droplets of this third phase may affect the gas to liquid mass transfer rate.

In systems that not inherently consist of three different phases, gas-liquid mass transfer (and thus the production rate) can be affected or even enhanced by the presence of a dispersed liquid phase with a higher dissolution capacity for the component to be transferred. This is the case in some biochemical applications in which an oil phase is deliberately used to enhance the mass transfer rate of oxygen to a water phase containing micro-organisms (Rols et al., 1990).

The mechanism of mass transfer in these systems is not well understood. As early as in 1970 (Yoshida et al., 1970), it was shown that one dispersed phase (toluene) can enhance mass transfer (after a decrease in the mass transfer rate at low dispersed phase fractions) whereas another dispersed phase (kerosene) decreases mass transfer, while both organic phases have more capacity for oxygen dissolution compared to the aqueous, continuous phase. In the study of Yoshida et al. (1970) (and in most other research studies on mass transfer in gas-liquid-liquid systems) the mass transfer rate is reported and determined via the measurement of the lumped volumetric mass transfer coefficient, k_La. This example indicates that, because of the complex influence of the dispersed phase fraction on k_L as well as on a (Cents et al., 2001), also in gas-liquid-liquid systems k_L and a should be measured individually and preferably simultaneously, to be able to analyze the effects of a dispersed phase on gas-liquid mass transfer, which will lead to a better understanding.

In this paper experiments will be presented, in which the volumetric mass transfer coefficient (k_La) is measured simultaneously with local values of the interfacial area (a_{local}) and the gas hold-up (ε_{local}). These values can be integrated to overall values ($< a >$) and ($< \varepsilon >$). For coalescing and non-coalescing electrolyte gas-liquid systems these results are compared with similar experiments in the literature. In addition, experiments were performed in a gas-water-toluene system in which also, k_La, a_{local}, $< a >$, ε_{local} and $< \varepsilon >$ were determined at different dispersed phase fractions. The droplet size, which may be an

important parameter in the mechanism that causes the enhancement of mass transfer, was determined in situ. In this way an attempt is made to increase the insight in influence of a second liquid phase on gas-liquid mass transfer and hydrodynamics.

2 MEASUREMENT TECHNIQUES

2.1 Gas-liquid interfacial area and bubble size distribution

Measurement of the local gas-liquid interfacial area and the bubble size distribution was performed using ultrasonic spectroscopy (Cents et al., 2004).The experimental technique is based on the difference in ultrasonic wave propagation in a dispersion of particles (solid particles, gas bubbles or liquid droplets) compared to propagation in the continuous liquid. The ultrasonic velocity (c) and attenuation coefficient (α) of a multi-phase system are directly related to the physical properties of the individual phases (e.g. density, compressibility). They are also dependent on the size and volume fraction of the particles and the frequency of the transmitted wave. The theory of ultrasonic propagation in multi-phase systems with an ensemble of particles was first derived by Epstein and Carhart (1953) and Allegra and Hawley (1972). The ultrasonic velocity and the attenuation coefficient are defined as:

$$c = \frac{d}{t} = \frac{d}{d/c_w(T) + \Delta t} \tag{1}$$

$$\alpha = \frac{-\ln\left(I_\varepsilon / I_w\right)}{d} + \alpha_w(T) \tag{2}$$

Both quantities are difficult to measure directly, but have to be determined in reference to a single solvent, which was water in the present study (c_w and α_w). Both properties are strongly dependent on temperature and therefore the temperature needs to be known accurately ($\pm$ 0.05 K). In these equations d is the path length of the measurement, I_w and I_ε are the intensities in the continuous phase and in the dispersion respectively. Δt is the time difference between the signal that has travelled through the dispersion and a reference signal (that has travelled the same distance through the continuous phase). More details of the method are described in section 3.

In Figure 1 the effect of increasing gas-liquid interfacial area on the attenuation coefficient is shown. The attenuation coefficient increases with increasing interfacial area and the relationship is linear in the high

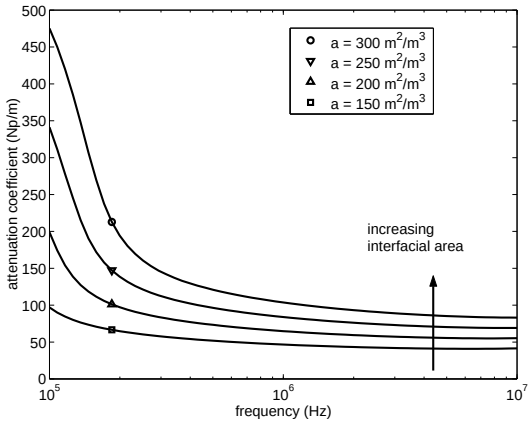

Figure 1: Attenuation coefficient as function of the interfacial area. $\varepsilon = 0.08$, $\sigma = 0.1\mu$.

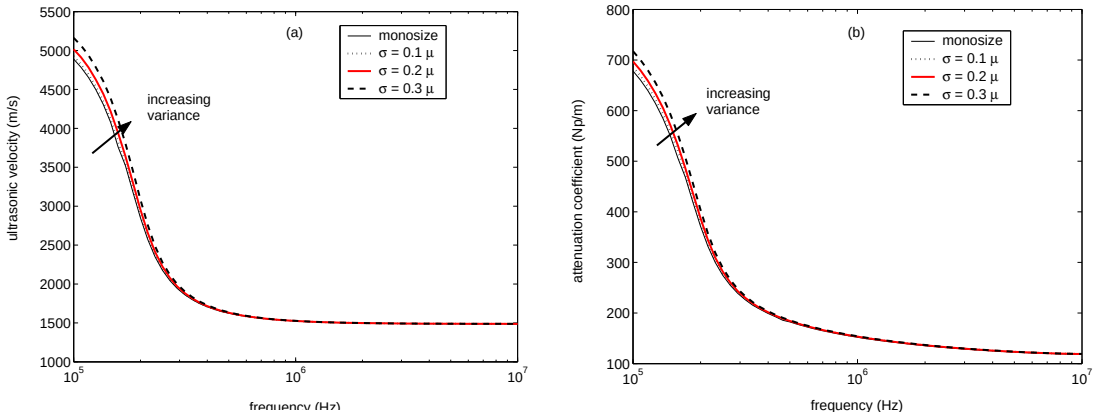

Figure 2: Influence of the width of the log-normal distribution on the ultrasonic velocity and attenuation coefficient. $\varepsilon = 10\%$, $d_{32} = 1.4$ mm in all cases.

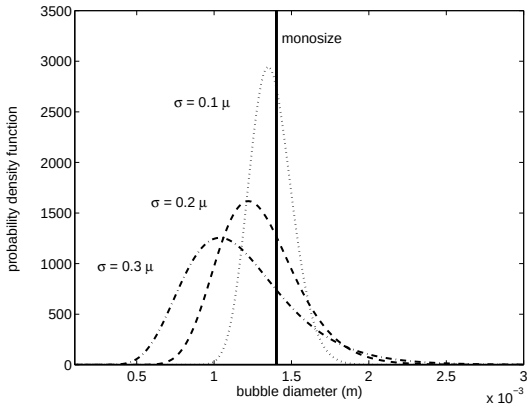

Figure 3: Log-normal distributions used in the calculations. d_{32} is 1.4 mm in all cases.

frequency regime and will approach $a = 4\alpha$ at infinite values of the product of frequency and bubble radius. In Figures 2a and 2b it is shown that in the high frequency regime (> 1 MHz) the ultrasonic velocity and the attenuation coefficient are independent of the bubble size distribution (assuming that the distribution is small enough to exclude very small bubbles ($<< 100\mu$m), as these bubble cause a dependence on the size distribution at higher frequencies). This means that at the high frequencies measurement of the interfacial area is possible at a single frequency (at lower frequencies this is not possible as multiple solutions will exist for different interfacial areas and different size distributions). Especially in case of mapping the local interfacial areas over an entire reactor volume, this saves a lot of time performing the experiments.

Figure 2 also shows that it is possible to determine the width of the distribution mainly in the low frequency (< 1 MHz) regime. However, it is shown by Cents et al. (2004) that it is desirable that the local gas hold-up is known, because multiple solutions yielding the same interfacial areas may exist. Furthermore, the attenuation coefficient is not very sensitive to the variance in the log-normal distribution. While the differences of the distribution widths that are used in Figures 2a and 2b (the used distributions are presented in Figure 3) are large, the values of the ultrasonic velocity and the attenuation coefficient both differ maximally 10%. With accurate measurements, however, it is possible to determine the width of the distribution in the low frequency regime.

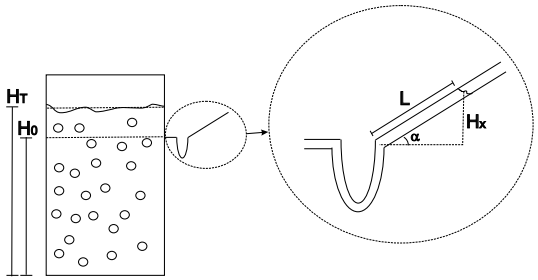

Figure 4: Inclined tube method for measurement of the overall gas hold-up.

2.2 Gas hold-up

Electrical conductivity was used for the measurement of local gas hold-up at different positions in the reactor. Details of the method are presented elsewhere (Cents et al., 2004).

The overall gas hold-up can be determined by measurement of the total liquid height in the reactor with and without gas sparging respectively, according to:

$$\varepsilon = \frac{V_G}{V_T} = \frac{V_T - V_L}{V_T} = 1 - \frac{H_0}{H_T} \tag{3}$$

In opaque vessels and in vessels in which height reading is difficult due to a large amount of turbulence induced by a stirrer, an alternate method for the determination of the overall gas hold-up is necessary. For this reason the overall gas hold-up is measured using the method proposed by Meng et al. (2002), which makes use of an inclined tube outside the vessel at the liquid height without sparging (H_0, see Figure 4). These authors obtained accurate results with this method compared to a gamma ray density monitoring system. To stabilize the liquid surface in their inclined tube a known amount of oil was put on top of the surface. This part was not used in this work, because of the risk of contamination of the continuous water phase. The tube is curved at the bottom side to prevent entrance of air bubbles and the measurement tube is put in an angle to improve the accuracy of the measurement.

The gas hold-up is calculated by equating the pressure in the inclined tube to the hydrostatic pressure in the vessel ($\Delta p^{ves} = \Delta p^{it}$). Making use of $\Delta p = \rho g \Delta H$ this results in:

$$\rho_{GL} g \left(H_T - H_0\right) = \rho_L g H_X \tag{4}$$

By making use of Equation 3, H_T can be written as $H_0/(1-\varepsilon)$. Because ρ_{GL} equals $(1-\varepsilon)\rho_L + \varepsilon\rho_G$, Equation 4 results in:

$$H_0 \frac{\varepsilon}{(1-\varepsilon)} \left((1-\varepsilon)\rho_L + \varepsilon\rho_G\right) = \rho_L H_X \tag{5}$$

From this equation the gas hold-up can be obtained as:

$$\varepsilon = \frac{\left(H_0 + H_X\right)\rho_L - \sqrt{\rho_L^2 \left(H_0 - H_X\right)^2 + 4 H_0 H_X \rho_L \rho_G}}{2 H_0 \left(\rho_L - \rho_G\right)} \tag{6}$$

Note that this result is different compared to the erroneous equation in the work of Meng et al. (2002). When the gas phase consists of air at room temperature and atmospheric pressure the gas phase density can be neglected and Equation 6 simplifies to:

$$\varepsilon = \frac{H_X}{H_0} = \frac{L\sin(\alpha)}{H_0} \tag{7}$$

This simplification results in a maximum relative error of 0.05% up to 30% gas hold-up. A possible introduction of error in this method occurs when the gas hold-up in the top part of the vessel (the measurement part) is not equal to the hold-up in the bottom section. The magnitude of the error depends, on the average gas hold-up and the amount of deviation of the top part from the bottom part and is larger at higher average gas hold-ups and at higher deviations in the top section. However, at the maximum gas hold-up applied in the stirred vessel in this work (13%) and in case the gas fraction in the top part is 50% less compared to the average value the relative error is still only 7%, which is quite acceptable in comparison with plain visual height reading in a turbulent stirred vessel.

2.3 Volumetric mass transfer coefficient

The volumetric mass transfer coefficient is determined using the dynamic oxygen method. In this method the response to a step change in the gas phase oxygen concentration is measured by an oxygen meter in the liquid phase. Furthermore, the diffusion of oxygen in the measurement probe time has to be taken into accountant when the probe response time, τ_P, $>> 1/(5k_La)$.

2.3.1 Mathematical model: The determination of the volumetric mass transfer coefficient requires the use of appropriate models for the mixing in liquid and gas phases. Linek et al. (1987) and earlier van 't Riet (1979) have pointed out that especially for high values of the gas phase residence time it is necessary to take the change in gas phase concentration during the measurement into account. Furthermore, the following assumptions were made:

1. Both the gas phase as well as the liquid phase are well mixed.
2. The probe responds as a first order system and the characteristic probe time is τ_P
3. The counterdiffusion of nitrogen can be neglected. This was verified by Linek et al. (1982)
4. The hydrodynamics in vessel remain unchanged during the interchange of gases with a different composition.
5. The gas flow rate, Φ_G, is constant.

This then results in the following oxygen mass balances:

Gas phase:

$$\frac{dc_G}{dt} = \frac{(c_{G,in} - c_G)}{\tau_G} - k_La(mc_G - c_L)\frac{V_L}{V_G} \tag{8}$$

Liquid phase:

$$\frac{dc_L}{dt} = k_La(mc_G - c_L) \tag{9}$$

Diffusion in the probe:

$$\frac{dc_P}{dt} = \frac{(c_L - c_P)}{\tau_P} \tag{10}$$

At time $t = 0$ the concentrations are: $c_G = c_{G,in}$, $c_L = 0$ and $c_P = 0$.

The solution of this system of three coupled linear differential equations must be compared with the experimental liquid phase concentration to obtain the volumetric mass transfer coefficient. This can be accomplished by moment analysis of both the probe and the liquid phase response according to Dang et al. (1977). Although this method is substantially simpler compared to curve regression methods, wrong absorption curves are not recognized easily (Linek et al., 1987), which can lead to errors in the estimated k_La values. Therefore the experimentally obtained liquid phase concentrations are regressed to the liquid phase concentration as determined by the mathematical model using a Nelder-Mead simplex optimization (Nelder and Mead, 1965). To accelerate the optimization process an analytical solution to the system of differential equations is derived.

3 EXPERIMENTAL SET-UP

The experimental set-up consists of a reaction vessel, which is 40 cm in diameter and the operational amount of liquid was 52.6 liter when water was used as the continuous phase and 42.6 liter in the experiments with electrolyte solutions. The reactor was equipped with a 6-bladed Rushton turbine with a diameter of one third of the reactor diameter (13.3 cm) and that was placed at 13.3 cm from the bottom. The blade width of the stirrer was 27 mm (1/5 of the impeller diameter). The turbine was driven by a motor with a variable stirring speed with a maximum speed of 960 rev/min. Four baffles of 4 cm in diameter ensured adequate mixing inside the vessel. The gas is sparged in the vessel through two 8 mm holes (30 mm apart) in the bottom of the reactor at 13 cm below the impeller. A schematic diagram of the used set-up is presented in Figure 5.

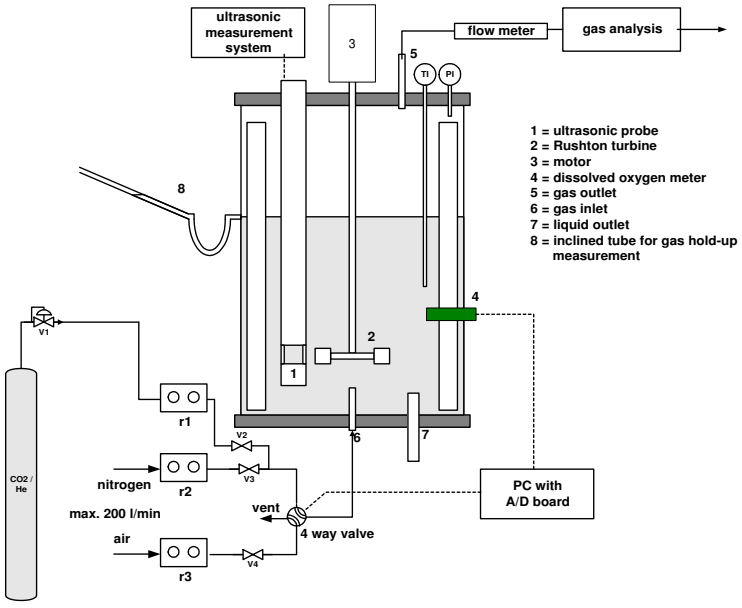

Figure 5: Experimental set-up for simultaneous measurement of k_La using the dynamic oxygen method and the interfacial area using ultrasonic spectroscopy.

3.1 Measurement of interfacial area, gas hold-up and bubble and droplet size distribution

The experimental set-up (Figure 6) consists of an arbitrary waveform generator (AWG), which transmits any desired electric signal to a piezoelectric transducer (T). The transducer converts the electric signal to a pressure wave that is received in a second transducer (R) where the latter is converted back into an electric signal, which is acquired with a digital oscilloscope. Simultaneously, a trigger signal is transmitted to the oscilloscope assuring that in every measurement the starting point, $t = 0$, is known accurately. A tone-burst signal, a limited number of cycles of a certain frequency, is used for determination of the velocity and the attenuation coefficient, which has the advantage of a low power input and the absence of signal disturbances (which may not be the case using continuous signals). The time difference between the signal in the dispersion and the reference signal can be determined using a cross-correlation function, which is also shown in Figure 6. To be able to measure small droplets as well as larger gas bubbles a frequency range of 100 kHz-100 MHz can be covered.

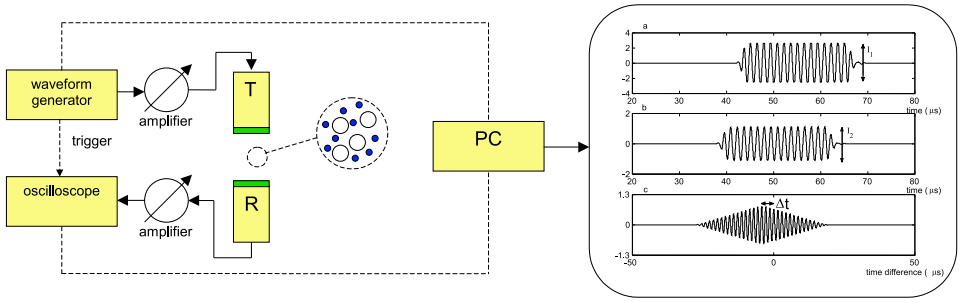

Figure 6: Set-up of the ultrasonic measurement system and signal analysis in the PC.

The sending and receiving transducers were placed in a stainless steel probe of 50 mm in diameter with a variable distance between the transducers with a maximum of 50 mm. Due to the fact that the transducers that transmit the low frequencies were much larger (33 mm) in outer diameter compared to the the high frequency transducers (12 mm), the transducers were covered with a steel jacket to ensure that the probe had a similar shape under all conditions applied. Furthermore, the probe was designed to cause the least disturbance to the gas-liquid flow pattern as possible. Only three stainless steel rods of 4 mm connected the transmitting and receiving part of the probe. The coaxial wiring from the transducers to the electrical equipment was stored inside the probe (through the connection rods). The probe could be positioned very accurately (within 0.3 $^\circ$ and 0.5 mm, respectively) and the distance between the transducers could be changed from the outside of the vessel using a rotational scaling device.

The probe for the measurement of the dispersed phase hold-up was constructed of PVC with stainless steel electrodes. The distance between the electrodes was fixed at 50 mm. The stainless steel connection rods were covered with a teflon coating to prevent disturbances by conduction through these rods. Also the inside reactor wall and the connection between the Rushton turbine and the motor were insulated to prevent short-circuiting of electrical current.

3.2 Volumetric mass transfer coefficient

For the determination of the volumetric mass transfer coefficient a 4-way valve was used, which was designed for fast ($<$ 100 ms) switching between air and nitrogen. Both the flows were controlled by flowmeters with a maximum of 200 liters per minute. The gas flow that was selected for the measurements in water and water containing different amounts of toluene was 40 l/min. The tubing between the valve and the vessel was 1.5 meter long and had an inner diameter of 10 cm, which means that the time between for the gas to reach the vessel was 0.2 seconds. This time was taken into account in the calculation of the results. The liquid phase oxygen concentration was measured using a Lazar Labs dissolved oxygen meter with a teflon membrane.

This membrane has a somewhat higher response time (6.7 seconds), but has the advantage of being resistant to toluene. The probe time was measured by rapidly dropping the oxygen probe in an environment with a different oxygen concentration, while measuring the response of the probe and was somewhat higher than the value given by the manufacturer (5.5 seconds).

3.3 Gas phase residence time

Measurement of the gas phase residence time distribution was performed by making use of ultrasound (Cents et al., 2003). Helium was added to the nitrogen stream (step-function) and the response at the outlet of the reactor was determined by making use of the difference in the ultrasonic velocity in helium compared to nitrogen. The trigger to switch the valve was sent by the oscilloscope and in this way the starting point, $t = 0$, is always perfectly known.

4 MAPPING OF LOCAL VALUES

To obtain a complete profile of local values, measurements were performed in the mid-plane between two adjacent baffles at 13 well-defined positions in the reactor. The measurement frequency that was used for the ultrasonic technique was 2 MHz. The probe was inserted from the top of the reactor, where the angle and depth of the probe define the positions in the tank (see Figure 7). The measurement points were selected to cover a region as large as possible. X12 and X13 have a slightly different horizontal coordinate, because of the curvature of the bottom of the vessel and because there was hindrance of the stirrer. For this reason a (small) part of the bottom region of the vessel could not be reached.

The overall values of the interfacial area and the gas hold-up can be calculated by integration over the reactor volume, assuming rotational symmetry. Each point in the vessel represents a certain volume V_i, which is defined by its spatial coordinates. The measurements points are defined as the exact mid points of the space between the transducers and the volumes they represent are calculated as $V_i = \pi \Delta r^2 \Delta H$. The volume that could not be reached was omitted from the calculation (see Figure 8). This results in loss of information of the bottom of the tank and very close to the impeller. For every measurement point a certain volume fraction can now be calculated, $f_i = V_i / \sum_i V_i$. The integration method did not influence the results for the overall values to a large extent compared to normal averaging. The overall values for the interfacial area, the gas hold-up and the Sauter diameter can be determined:

$$\langle a \rangle = \sum_{i=1}^{13} a_{local,i} f_i \tag{11}$$

$$\langle \varepsilon \rangle = \sum_{i=1}^{13} \varepsilon_{local,i} f_i \tag{12}$$

$$d_{32} = \frac{6 \langle \varepsilon \rangle}{\langle a \rangle} \tag{13}$$

The Sauter diameter can also be calculated using the overall gas hold-up as measured with the inclined tube. Ideally the two methods to determine $< \varepsilon >$ would give the same results.

The inclined tube had a total height of 10 cm, so it could be used up to almost 20% of gas hold-up. The angle of the tube was chosen to be 23°, which increased the measured length of the liquid (and thereby the accuracy) with a factor 2.5 compared to a vertical tube.

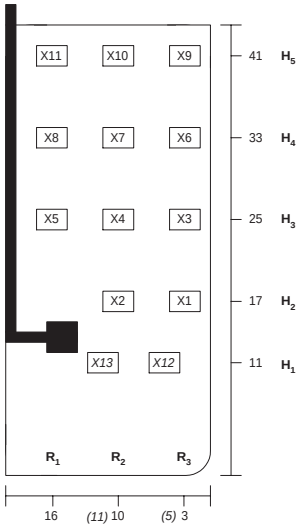

Figure 7: Positions in the reactor (dimensions are in centimeters)

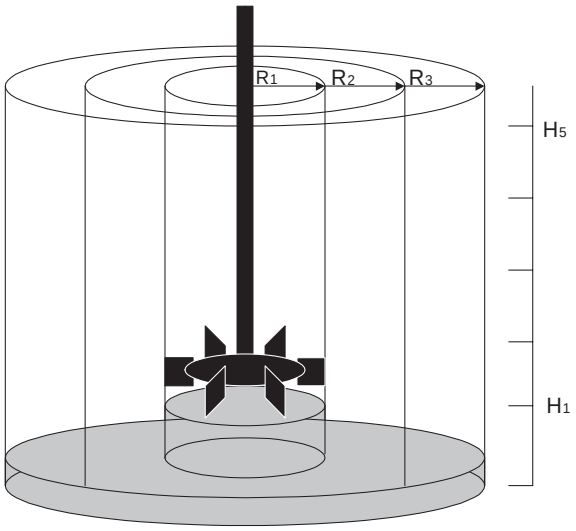

Figure 8: Schematic representation of the method to integrate local values to average values in the vessel. (The grey area is not used in the integration).

5 RESULTS AND DISCUSSION

5.1 Validation of gas hold-up methods

To check the validity of both methods for the measurement of the overall gas hold-up using the inclined tube and the method for determination of the local gas hold-up using electrical conductivity, a cross-validation of both methods was performed. The experiments were performed in the small bubble column, in which a porous plate gas disperser assured a nice homogeneous flow pattern so that local and overall gas hold-up are comparable. The column was 15 cm in diameter and 25 cm in length and the measurement position was 15 cm above the distributor. Also standard height reading was possible due to the homogeneous flow and the non-turbulent surface. Tap water was used as the liquid phase to allow the conductivity technique to work optimally. The results of the three methods are presented in Figure 9.

As is shown in Figure 9 the agreement between the three methods is very good. The maximum relative deviation from the average is 7.6 % and the average relative deviation is 3.6 % and the error seems to be randomly oriented. This result shows that the inclined tube method as well as the conductivity method can be used for gas hold-up measurement in the stirred vessel.

5.2 Validation of the ultrasonic technique

In order to test the technique for the measurement of bubble size more extensively, a comparison of ultrasonic spectroscopy with a digital camera technique was performed. The bubble size was measured in a flat (20x3x150 cm) bubble column using the ultrasonic technique in combination with the electrical conductivity method and using a digital camera technique with digital image analysis, simultaneously. The camera was placed 10 cm in front of the column and the ultrasonic transducers were mounted into the wall of the column (the measurement path length was 20 cm). Measurement of the exact size distribution using the ultrasonic technique was difficult, mainly due to the small attenuation and ultrasonic velocity differences. These differences were small due to low gas hold-ups that were applied ($\approx 1\%$), which was necessary for the digital camera technique to work optimally. It was, however, possible to determine the Sauter mean bubble diameter by simultaneous measurement of the interfacial area and the gas hold-up using the electrical conductivity

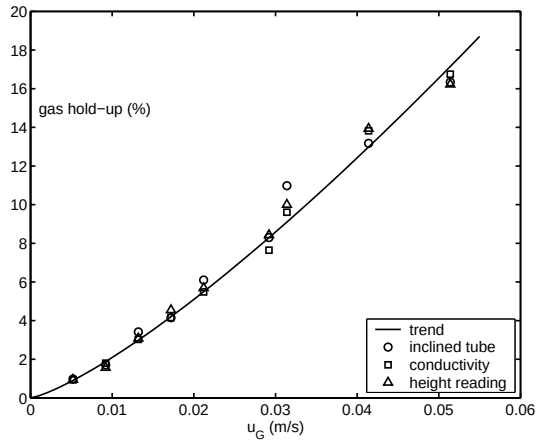

Figure 9: Cross-validation of different methods for gas hold-up measurement.

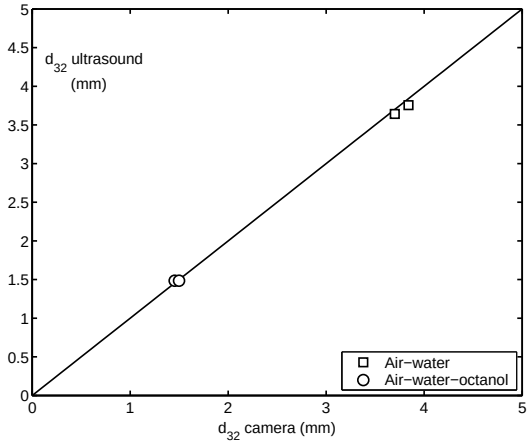

Figure 10: Parity-plot of the Sauter mean diameter obtained with the ultrasonic technique and with a digital camera technique.

technique. As can be seen in Figure 10 a good agreement between the two methods was obtained for coalescing (air-water) and non-coalescing (air-water-0.5 g/l octanol) systems, respectively.

5.3 Influence of the ultrasonic technique

5.3.1 Ultrasonic power input: It is very important that the influence of the power input due to the transmission of the ultrasonic waves does not influence the bubble size distribution between the transducers. A high power input can cause breakage of bubbles and can result in unwanted cavitation. In this work, however, the power input was kept very low (< 0.005 W), as a tone burst operation with a 20 Hz signal frequency was used.

The applied ultrasonic power input was very small compared to the power generated by the stirrer and can therefore safely be neglected. To validate that the bubbles between the transducers were not affected by the ultrasonic power input the attenuation coefficient, which has an almost linear relationship with the gas-liquid interfacial area, was measured under different applied power inputs and further identical conditions. The results are presented in Figure 11 and show that there is hardly any influence of the power input. The maximum deviation from the average is 7%, which is most likely within the experimental error.

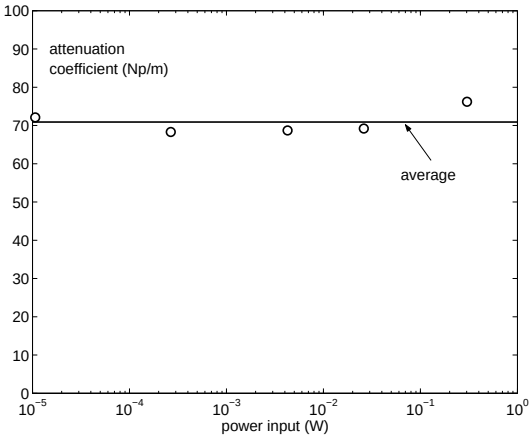

Figure 11: Influence of the power input added by the ultrasonic probe on the measured attenuation coefficient. Position: X4, frequency: 300 kHz, Stirring speed: 640 rpm, Superficial gas velocity: 0.58 cm/s.

5.3.2 Ultrasonic probe: As the probe was quite large compared to the reactor size, the results as obtained with the above described measurement probe were compared with another probe. This test probe was completely open, but also less stable when exposed to the turbulence in the reactor. The differences in the results with the two probes were always small (relative deviations less than 10 %). The results of the solid probe had a better reproducibility com-

pared to the open probe, mainly due to the good stability under high turbulence in the vessel. Furthermore, this probe could be put at its correct angle and immersion depth very accurately (within 0.3 ° and 0.5 mm, respectively). It is therefore concluded that the probe geometry did not significantly influence the results presented hereafter.

6 RESULTS IN COALESCING SYSTEMS

6.1 Values of interfacial area, gas hold-up and Sauter mean diameter

In Figures 12 to 16 the measured values of the local interfacial area, gas hold-up and the calculated Sauter diameter are shown for a system of tap water and air at a superficial velocity of 0.58 cm/s and stirring speeds of 200 - 960 rpm.

From these figures it can be concluded that gas dispersion in vessels containing coalescing media is highly inhomogeneous, which was already observed by Calderbank (1958). The gas-liquid interfacial area is the highest in the impeller discharge zone (X12, X13) and is much lower (a factor 4 at high stirring speeds) in the upper part of the reactor. Furthermore, the difference between the center and the wall part of the reactor is quite large, mainly in the vertically middle part of the vessel. Large gas hold-ups are found mostly in the center of the reactor approximately 12 cm above the impeller. At the wall the gas hold-up is lower and the bubbles are smaller, which is probably caused by the typical flow pattern in a Rushton turbine agitated vessel. The energy dissipation is much higher in the impeller zone compared to the rest of the vessel, which causes the formation of small bubbles. Also the velocity of the liquid is very high in the impeller discharge zone, which is the reason that relatively low gas hold-ups are observed in this region. The direction of flow is from the impeller to the wall (see Figure 17c-e) and these small bubbles are transported in this direction with a still relatively high speed. The bubbles on positions X1 and X3 are therefore quite small and the gas hold-up is still rather low (while the interfacial area is large !) on these positions. These effects were also observed (to a lesser extent) by Barigou and Greaves (1992), Barigou and Greaves (1996) and Alves et al. (2002).

To compare the present results with other data in literature radially averaged axial profiles were constructed of the gas liquid interfacial area, the gas hold-up and the Sauter mean diameter in the same way as was done by Calderbank (1958) and Barigou and Greaves (1996). The results of the interfacial area are presented in Figure 18 and show that the highest interfacial area is observed in the impeller plane. Furthermore, a small increase in interfacial area is observed in the plane at 25 cm from the bottom of the

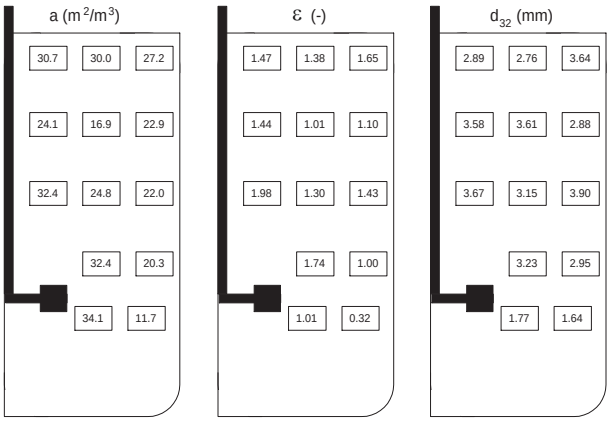

Figure 12: Values of interfacial area, gas hold-up and Sauter mean diameter at a stirring speed of 200 rpm and a superficial gas velocity of 0.58 cm/s.

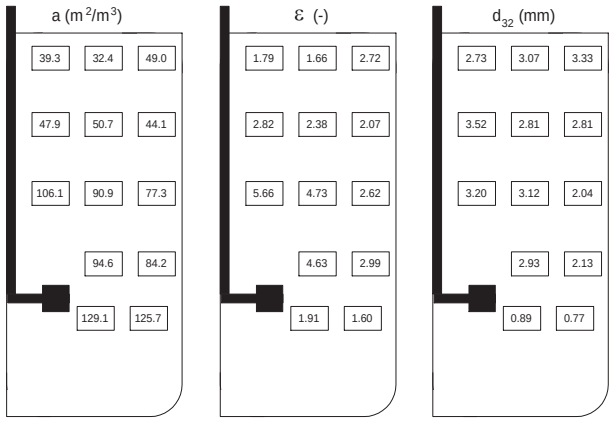

Figure 13: Values of interfacial area, gas hold-up and Sauter mean diameter at a stirring speed of 420 rpm and a superficial gas velocity of 0.58 cm/s.

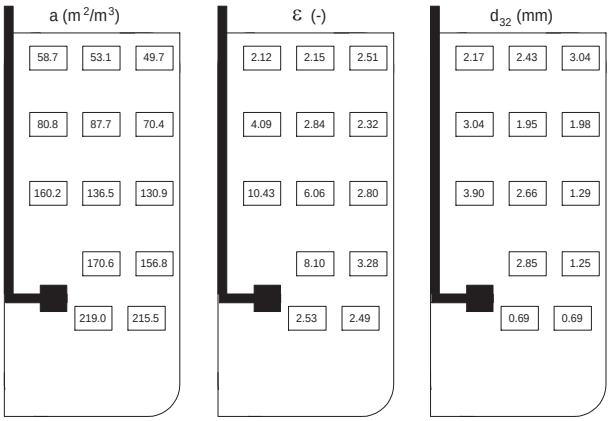

Figure 14: Values of interfacial area, gas hold-up and Sauter mean diameter at a stirring speed of 640 rpm and a superficial gas velocity of 0.58 cm/s.

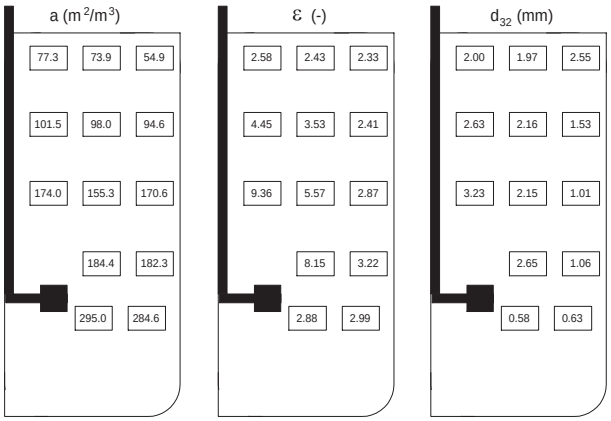

Figure 15: Values of interfacial area, gas hold-up and Sauter mean diameter at a stirring speed of 770 rpm and a superficial gas velocity of 0.58 cm/s.

tank, which was due to the increased gas hold-up in this plane. The results are in reasonable agreement with the results from Calderbank (1958), who used a light scattering technique. The main difference between their work and this work is that the peak in interfacial area above the impeller plane is much smaller in our case. As it is clearly shown in Figure 18 the interfacial area increases with the stirring speed at all places in the reactor.

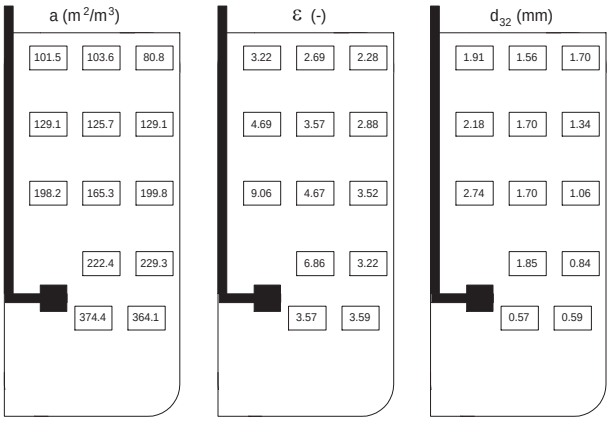

Figure 16: Values of interfacial area, gas hold-up and Sauter mean diameter at a stirring speed of 960 rpm and a superficial gas velocity of 0.58 cm/s.

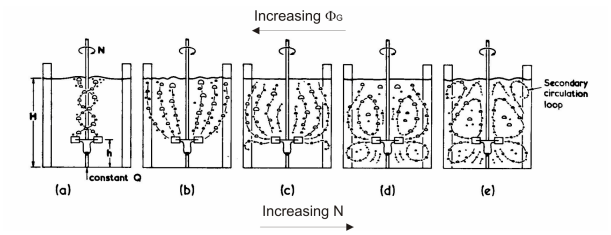

Figure 17: The five characteristic stages of gas dispersion defined by Nienow et al. (1977) (a) partial bubble column; (b) full bubble column; (c) onset of dipsersion in the lower part; (d) complete circulation; (e) secondary circulation.

The gas hold-up profile, which is shown in Figure 19 is quite similar to the work of Calderbank (1958), who made use of a 500 cm^3 glass bulb with a gas burette attached to it. In their study, local sampling was performed by opening and closing a stopcock and the gas hold-up was determined afterwards by measurement of the gas and the liquid volume. Both in this work and in their work the main part of the gas hold-up is situated in the area approximately 2/3 of the clear liquid height from the bottom. The results are somewhat different compared to the work of Barigou and Greaves (1996), who used a contact conductivity probe that measured the time of probe tip touching the gas compared to the time that the probe tip touched the liquid phase. These authors also measured a larger gas hold-up in the region above the impeller compared to impeller plane itself, but the gas hold-up profile in the top region of the tank

was quite flat, while in our work and in the work of Calderbank (1958) the hold-up in the upper part was significantly lower compared to the middle part. A reason for this might be the fact that Barigou and Greaves (1996) used a vessel with the impeller at 1/4 of the clear liquid height above the bottom (1/3 in this work), which induces less turbulence in the upper part of the reactor. Because Barigou and Greaves (1996) calculated the interfacial area from measurement of the gas hold-up and the bubble size distribution, these values differed from the interfacial areas in this work in the same way.

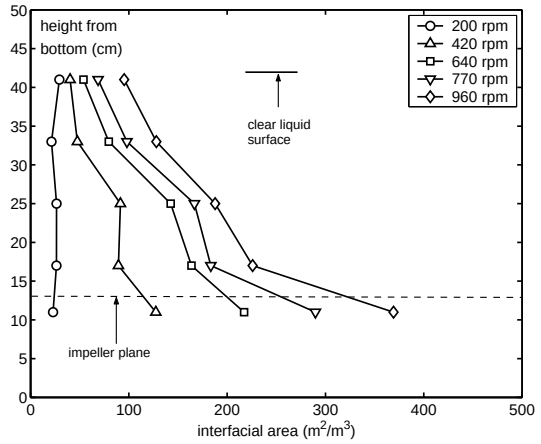

Figure 18: Vertical profiles of the gas-liquid interfacial area at different impeller speeds.

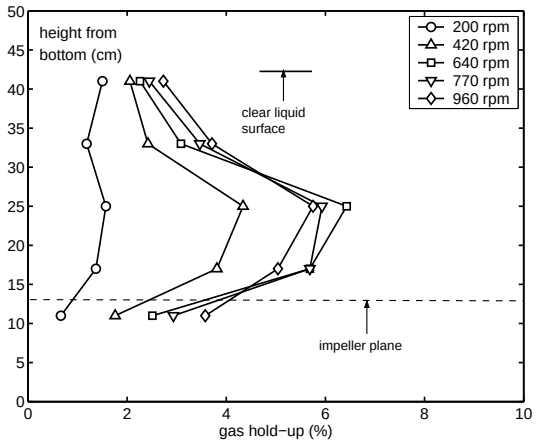

Figure 19: Vertical profiles of the gas hold-up at different impeller speeds.

The vertical distributions of the Sauter mean diameter as a function of the impeller speed are presented in Figure 20. The patterns are very similar for each stirring speed and show a low diameter in the impeller discharge zone and the diameter is increasing to an approximately constant diameter above 25 cm from the bottom. These trends are quite similar compared to the trends obtained by Barigou and Greaves (1992), who made use of a capillary suction probe for measurement of the bubble size distribution. At the lowest impeller speed the bubbles coalesce after they leave the impeller discharge zone at 1.7 mm to reach a value of approximately 3.5 mm. At the highest impeller speed (960 rpm) the bubble size increased from 0.6 mm to reach a maximum value of 1.8 mm (radially averaged). The values for the bubble size as shown in Figures 12 to 16 are predominantly increasing while going along the liquid flow pattern as explained in Figure 17d-e. The decreasing trend in the bubble diameter with increasing height at the lowest impeller speed is not logical from a physical point of view and might be due to experimental error.

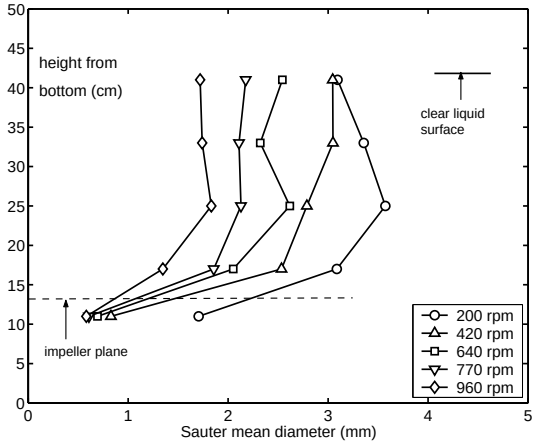

Figure 20: Vertical profiles of the Sauter mean diameter at different impeller speeds.

6.2 Influence of impeller speed

To show the influence of the speed of the impeller on the interfacial area and the gas hold-up at specific regions in the vessel, two different points are selected. X13, which represents the impeller discharge zone and X8, which represents the bulk of the vessel. The effect of the rotational speed on the interfacial area is shown in Figure 21a, which makes clear that the interfacial area is a stronger function of the impeller speed near the impeller ($a \sim N^{1.54}$) compared to the bulk ($a \sim N^{1.08}$). Furthermore, the large differences of the

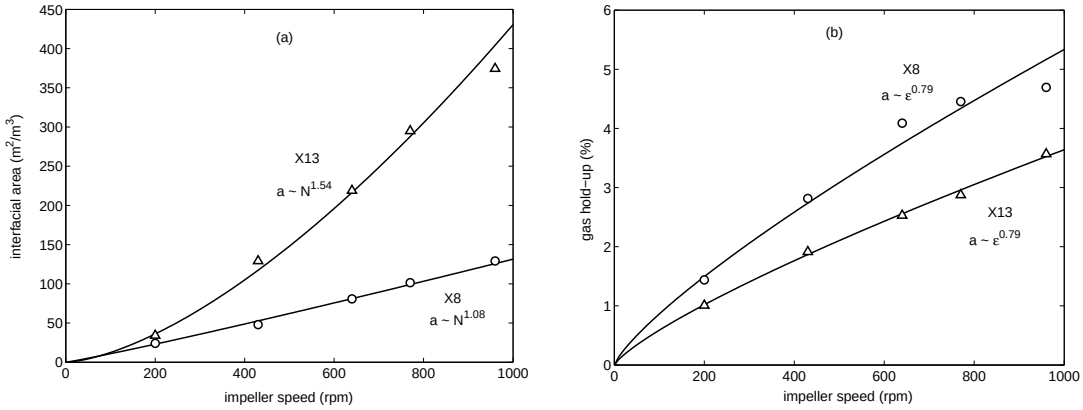

Figure 21: Influence of the impeller speed on the interfacial area (a) and on the gas hold-up (b) at two different places in the reactor. Solid lines represent the best fit through the experiments using a power law function.

absolute values of the interfacial area are clearly shown. In Figure 21b the effect of the impeller speed on the gas hold-up at X8 and X13 is presented. The gas hold-up in the center part of the vessel is higher compared to the region close to the impeller. Furthermore, the dependency of the gas hold-up on the stirring speed is similar in the bulk region and in the impeller region (exponent = 0.79), which indicates that the larger exponent in the interfacial area is due to a larger dependency of the bubble size on the impeller speed in the impeller region (-0.75 compared to -0.29). The explanation for these effects lies in the fact that the bubble size is determined by the relative speeds in which the coalescence and the break-up process take place. As the break-up process is relatively fast in the impeller region, the dependence of the bubble size on the impeller speed is larger in this region, which is reflected on the interfacial area.

6.3 Influence of superficial gas velocity

The influence of the superficial gas velocity was studied similar to the influence of the impeller speed at two positions, one close to impeller, X2, and one in the top region of the vessel, X10. The results indicate that the interfacial area increases with increasing superficial gas velocity, as can be seen in Figure 22. The area is a stronger function of the superficial gas velocity at low stirring speeds, which was also found by Mehta and Sharma (1971). The area is also a stronger function of the superficial gas velocity at positions close to the impeller. The exponents are somewhat lower compared to the work of Calderbank (1958),who predicted $a \sim u_G^{0.5}$, but are in reasonably good agreement with the work of Hughmark (1980), in which the exponent was 1/3. For a better comparison more work on the influence of the superficial gas velocity should be performed.

6.4 Integral values of the mass transfer parameters

The local values of the interfacial area, gas hold-up and Sauter mean diameter can be integrated according to the procedure described in 4 and are presented in Table 1. The Sauter mean diameter can be calculated in two different ways: on the basis of the integrated gas hold-up, $< \varepsilon >$, or based on the hold-up measurement using the inclined tube, ε_{incl}. This results in two different Sauter mean diameters, $< d_{32} >$ and $d_{32,incl}$, which ideally are equal. The results will be discussed separately in the next paragraphs and a comparison with similar experiments in the literature will be performed.

6.5 Interfacial area

To validate whether the gas-liquid interfacial areas that were obtained using the ultrasonic technique are in line with similar experiments in the literature, a comparison was made with a correlation from the generally accepted work of Calderbank (1958), who made use of a light scattering technique in a 5 liter and 100

Table 1: The overall values of the mass transfer parameters.

N (rpm)	$< a >$ (m^2/m^3)	$< \varepsilon >$ (%)	ε_{incl} (%)	$< d_{32} >$ (mm)	$d_{32,incl}$ (mm)
200	24.8	1.25	1.60	3.03	3.88
420	75.7	2.82	3.16	2.23	2.50
640	124.4	3.76	4.49	1.81	2.17
770	153.0	3.86	4.94	1.51	1.94
960	190.8	3.93	5.34	1.24	1.68

liter stirred vessel with standard dimensions and equipped with a Rushton turbine. These correlations are generally not based on the impeller speed, but on the power input done by the impeller under gassed conditions. The power input by the impeller under ungassed conditions is given by:

$$P = N_P \, \rho N^3 D^5 \tag{14}$$

On the introduction of gas in the reactor the power input to reach a certain impeller speed decreases. Calderbank (1958) correlated the ratio of the gassed power input and the ungassed power input, P_g/P, on the basis of the Flow number, $Fl = \Phi_G/(ND^3)$:

$$Fl < 0.035 \rightarrow \frac{P_g}{P} = 1 - 12.6Fl \tag{15}$$

$$Fl > 0.035 \rightarrow \frac{P_g}{P} = 0.62 - 1.85Fl \tag{16}$$

Calderbank used a maximum stable bubble diameter approach to correlate his experiments on the interfacial area. This maximum stable diameter was derived by balancing the viscous and surface tension forces with the dispersive turbulence forces. Assuming Kolmogoroff's theory of isotropic turbulence this leads to:

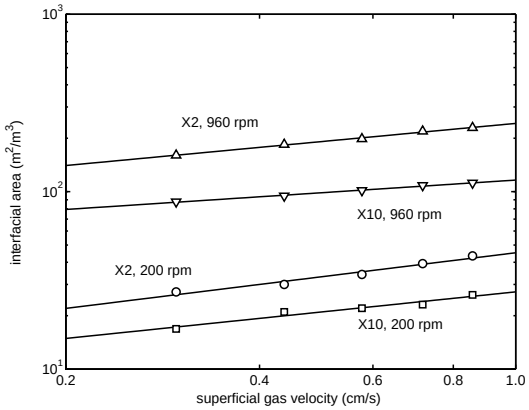

Figure 22: Influence of the superficial gas velocity on the interfacial area at two different places in the reactor and at two different impeller speeds. Solid lines represent the best fit through the experiments using a power law function. Exponents: X2 200 rpm: 0.45, X2 960 rpm: 0.34, X10 200 rpm: 0.38, X10 960 rpm: 0.24.

Table 2: Reactor dimensions and operating conditions.

parameter	symbol	value	dimension	remarks
tank diameter	T	0.40	m	
impeller diameter	D	0.133	m	
liquid volume	V	0.0526	m^3	in case of electrolyte solution: 0.0465 m^3
impeller blade width	W	0.026	m	
impeller blade length	L_B	0.033	m	
baffle width	B	0.04	m	
impeller height above bottom	H_I	0.133	m	
impeller power number	N_P	5.8	-	
diameter of the sparger	d_s	0.008	m	2 holes below the impeller
gas flow	Φ_G	$7.25 \cdot 10^{-4}$	m^3/s	unless specified otherwise

$$d = C_1 \left(\frac{\sigma_L^{0.6}}{\left(\frac{P_g}{V}\right)^{0.4} \rho^{0.2}} \right) \tag{17}$$

The gas-liquid interfacial area was measured using a wide variation of power input, surface tension and superficial gas velocity and correlated by this author to be:

$$a = 1.44 \left(\frac{\left(\frac{P_g}{V}\right)^{0.4} \rho^{0.2}}{\sigma_L^{0.6}} \right) \left(\frac{u_G}{u_T} \right)^{0.5} \tag{18}$$

In this equation u_T is the terminal rise velocity which was found to be constant (26.5 cm/s) for bubbles of 2-5 mm in water.

Hughmark (1980) correlated an extensive amount of data on flat blade impellers on the ratio of gassed and ungassed power input to give:

$$\frac{P_g}{P} = 0.10 \left(\frac{\Phi_G}{NV} \right)^{-1/4} \left(\frac{N^2 D^4}{W g V^{2/3}} \right)^{-1/5} \tag{19}$$

Both correlations for the gassed power input show, however, a completely different trend with respect to the impeller speed. The equations of Calderbank, (eq. 15 and 16) show an increasing trend with impeller speed, while the equation of Hughmark (19) shows a decreasing trend. For a fair comparison with the work of Calderbank the gassed power input of Calderbank was used, while the correlation of Hughmark is more generally accepted and the trend better represents the gassed power input as measured in this work. The used physical parameters and reactor dimensions are given in Tables 2 and 3.

The result of the comparison is presented in Figure 23 and shows that the interfacial area as measured in this work is in good agreement with the correlation of Calderbank, with an average absolute deviation of 10%. The interfacial area in this work can be well described with an equation of the form: $a \sim N^{1.32}$ (dotted line in Figure 23), while the exponent obtained with the correlations of Calderbank was 1.34. In the work of Hughmark (1980) an exponent of 1.23 was obtained, which is also in reasonable agreement with the exponent from this work. From these results it can be concluded that the measurement with the ultrasonic technique at the 13 selected positions gives an accurate representation of the overall gas-liquid interfacial area.

Table 3: Physical properties in water and in a 0.5 M K_2CO_3 / 0.5 M $KHCO_3$ buffer solution at 25 ° C.

parameter	symbol	value in water	value in buffer	dimension
density	ρ	997	1084	kg/m^3
surface tension	σ_L	72	74	10^3 N/m
liquid viscosity	μ_L	0.91	1.11	10^3 Pa s
gas viscosity	μ_G	1.8	1.8	10^5 Pa s
gravitational constant	g	9.81	9.81	m/s^2

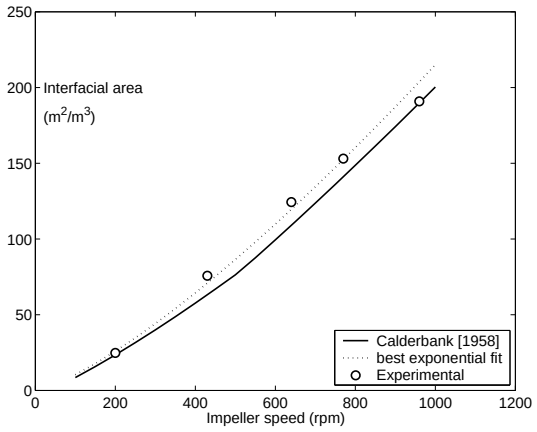

Figure 23: Comparison of the measured interfacial area using ultrasonic spectroscopy with the correlation of Calderbank (1958).

6.6 Gas hold-up

A comparison with literature correlations on the overall and local gas hold-up is difficult, because of the large scatter in the reported experimental data. This scatter can only be partly accounted for by the experimental error. Also the various flow regimes that can occur in a stirred vessel can be very important. Warmoeskerken and Smith (1985) performed an extensive study on the gas loading of disc turbine impellers and have clearly identified different regimes in terms of cavity formation behind the impeller blades:

1. loaded impeller with six vortices or six clinging cavities
2. loaded impeller with stable alternate larger and smaller cavities
3. flooded impeller with 6 clinging or six ragged cavities

According to the criteria of Warmoeskerken and Smith (1985) the experiments in this work at the three highest impeller speeds (640, 770, 940 rpm) are in the regime 1, the experiments at 200 and 420 rpm are in regime 2.

A comparison will be made with the work of Greaves and Barigou (1990), because these authors measured the gas hold-up and correlated the results for the different flow regimes. Their experiments were performed in a stirred vessel of 1 meter in diameter, equipped with a Rushton turbine, at 5 vertical positions, using a contact conductivity technique. For regime 1 these authors found the following correlation for the gas hold-up:

$$\varepsilon = 3.85 N^{0.73} \Phi_G^{0.62} \left(\frac{D}{T}\right)^{1.64} \tag{20}$$

For regime 2 Greaves and Barigou (1990) found:

$$\varepsilon = 1.33 N^{0.60} \Phi_G^{0.44} \left(\frac{D}{T}\right)^{1.33} \tag{21}$$

Furthermore, a comparison will be made with the work of Calderbank (1958), who used a suction probe with a gas burette attached to it for the measurement of the gas fraction and obtained the following equation:

$$\varepsilon = \left(\frac{u_G \varepsilon}{u_T}\right)^{0.5} + 0.000216 \left(\frac{\left(\frac{P_g}{V}\right)^{0.4} \rho^{0.2}}{\sigma_L^{0.6}}\right) \left(\frac{u_G}{u_T}\right)^{0.5} \tag{22}$$

The results of the measured values of the gas hold-up by integration of the local values and the measured values using the inclined tube in comparison with the above mentioned correlations are presented in Figure 24. The obtained results with the inclined tube are in good agreement with the correlation of Greaves and Barigou (1990) for a loaded impeller with clinging cavities. Both the correlation of Calderbank (1958) and the correlation of Greaves and Barigou (1990) for a loaded impeller with alternate cavities gives somewhat higher (average 28%) gas hold-up results compared to the values obtained from the inclined tube method used in the present study. The suction method of Calderbank might be somewhat inaccurate, because it assumes that gas and liquid are drawn into the probe at the same rate, which is not necessarily true. The deviation is most pronounced at low stirring speed (200 rpm), which should be in regime 2 according to the work of Warmoeskerken and Smith (1985). A possible explanation for this is the fact that the stirring speed of 200 rpm is below the critical stirring speed according to the correlations of Westerterp et al. (1963) (367 rpm) and Nienow et al. (1977) (291 rpm). This means that the gas phase is not completely dispersed throughout the reactor, which might account for a lower gas hold-up after integration.

Furthermore, there is a difference between the measured gas hold-up with the inclined tube in comparison with the gas hold-up from the integration of the local values. The average relative deviation between the two methods is 19 % and this is specified per impeller speed in Table 25. This means that the 13 selected positions in the vessel are not covering the vessel sufficiently accurate for integration to the overall gas hold-up. This might originate partly from the fact that is was not possible to measure at the bottom of the vessel and closely above the impeller, where high gas hold-ups can be found, mainly at high stirring speeds, when full gas dispersion is achieved. Also the measurements at the wall (X1, X3, X6 and X9), which are very important due to their large volume fraction in the integration, were taken very closely to the vessel wall, where a steep decrease of gas hold-up was found. This can also account for a lower gas hold-up on integration.

6.7 Sauter mean diameter

The Sauter mean diameter of the gas bubbles was compared to the established correlation proposed by Calderbank (1958):

$$d_{32} = 4.15 \left(\frac{\sigma_L^{0.6}}{\left(\frac{P_g}{V}\right)^{0.4} \rho^{0.2}}\right) \varepsilon^{0.5} + 0.0009 \tag{23}$$

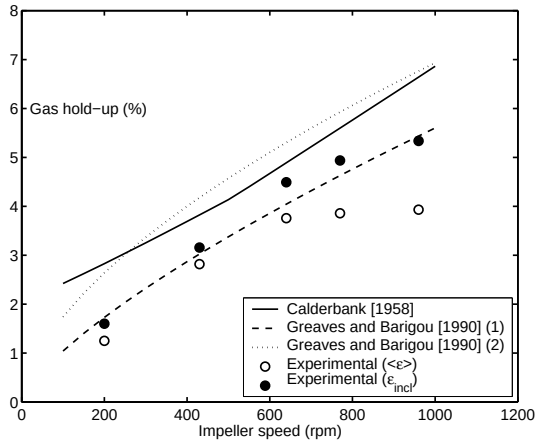

Figure 24: Comparison of the measured gas hold-ups using electrical conductivity with the correlations of Calderbank (1958) and Greaves and Barigou (1990).

impeller speed (rpm)	RD (%)
200	22
420	11
640	16
770	22
960	26

Figure 25: Relative Deviation (RD) between the different gas hold-up methods.

The Sauter mean diameter predicted by Calderbank is higher compared to the values measured in this work (Figure 26). This was to be expected, because similarly to this work, Calderbank calculated the Sauter mean diameter from measurements of a and ε. While the interfacial area was close to the area in this work, the gas-hold-up was significantly higher, resulting in a higher Sauter mean bubble diameter.

To establish correlations for the Sauter mean diameter Alves et al. (2002) measured bubble sizes at 29 different positions in a stirred vessel using a capillary suction technique. These authors divided the vessel into two regions: the bulk region and the impeller region. The data were combined with data from Martin (1995), Machon et al. (1997) and Bouaifi and Roustan (1998), who all used video/photography techniques and with data from Barigou and Greaves (1992), who used a capillary suction technique. For the bulk region the Sauter mean diameter was given by:

$$d_{32,bulk} = 0.0076 \left(\frac{P_g}{V} \right)^{-0.14} \tag{24}$$

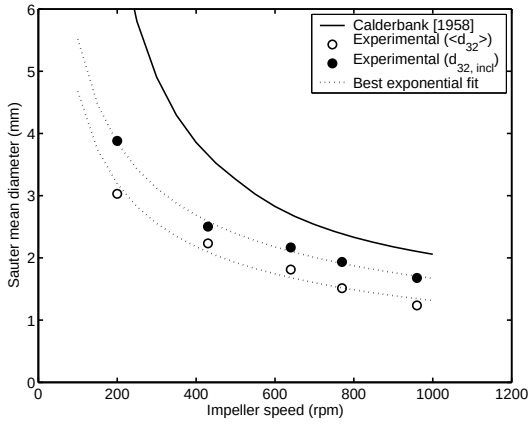

Figure 26: Comparison of the calculated Sauter mean diameter with the correlation of Calderbank (1958).

To compare the results obtained in the present study with Equation 24 the gassed power input was calculated using the relation of Hughmark (1980) (eq. 19) and the bulk region was represented by the positions (X1-X11). The exponent obtained in this work was -0.14, which is in exact agreement with the correlation. As expected the exponent is much lower compared to the exponent as predicted with the theory of isotropic turbulence (Eq. 17), which means that the bubble size is strongly influenced by coalescence in the bulk of the vessel. The pre-exponential constant in this work was 0.00685, which is only 10% lower compared to Equation 24.

Alves et al. (2002) gave the following expression for the Sauter meter in the impeller discharge zone:

$$d_{32,imp} = 8.5\left(1 + 32.5\frac{\Phi_G}{D^2}\right)\left(\frac{P_g}{V_{imp}}\right)^{-0.24} \tag{25}$$

The above correlation is not based on the total liquid volume, but on the impeller swept volume, $V_{imp} = 0.25\pi D^2 W$, which gives a better representation of the energy dissipated in the impeller zone. A comparison is made with the Sauter mean diameters in the impeller zone (X12, X13) determined in this work. The obtained exponent in this work was -0.245, which is in good agreement with Equation 25 and with the work of Lu et al. (1993) (-0.25). The pre-exponential factor was 17.1, which is somewhat lower (14%) than could be determined from Equation 25 (19.9).

From these results it can be concluded that Sauter mean diameters can be measured with a good accuracy using a combination of ultrasonic spectroscopy for measurement of the gas-liquid interfacial area and electrical conductivity for determination of the local gas-hold-up. Overall values are in reasonable agreement with the literature and the dependence on power input in different parts of the vessel are confirming literature results.

6.8 Mass transfer coefficients

The volumetric mass transfer coefficients are determined according to the method described in Section 3.2. The probe response time was determined by dropping the measurement probe very fast in a beaker with deoxygenated water and was found to be 6.7 sec, which is somewhat higher than specified by the supplier (5.5 s). In Figure 27 two probe response curves are plotted: (1) the response curve of the probe in the beaker with deoxygenated water (squares) and (2) a response curve of the probe in the vessel after switching from nitrogen to air at a superficial gas velocity of 0.58 cm/s and and a stirring speed of 640 rpm. The first part of curve 1, which is the most important part for the determination of the probe response time, is fitted by the mathematical model excellently. On the other hand, the curve shows some deviation from the trend of the mathematical model at high values of the normalized concentration, which might be due to the instability of dropping the probe manually in the beaker glass, which is less stable compared to the steady operation in the vessel. This is supported by the fact that the curve of the probe response concentration in the vessel (2), did not show any large deviations from the mathematical model. This means that the proposed mathematical model is sufficiently accurate to be used for k_La measurements in this system.

In Table 4 the volumetric mass transfer coefficients are presented at 430, 640, 770 and 960 rpm. The value at 200 rpm could not be determined due to sticking of air bubbles to the DO-probe, which led to erroneous determinations of the volumetric mass transfer coefficient. The mass transfer coefficients were averaged from a number of experiments (see Table 4, which consisted of 50% absorption and 50% desorption experiments. k_La_{abs} was on average 7% higher compared to k_La_{des}, which is comparable with the standard deviations in the measurements. This means that absorption and desorption are mirror image processes. Furthermore, the liquid phase mass transfer coefficient, k_L, could be calculated as the ratio of the volumetric mass transfer coefficient and the interfacial area as determined in the previous section. The value of the measured k_La coefficient was always larger than $1/(5\tau_P)$, but never exceeded $1/\tau_P$, which means that accurate measurement of k_La is possible, on the condition that the probe characteristics are taken into account.

Table 4: Mass transfer coefficients at different stirring speeds. u_G: 0.58 cm/s.

N (rpm)	nr. of exp. (-)	σ (%)	k_La (s^{-1})	a (m^2/m^3)	k_L (10^4 m/s)
420	4	2.6	0.034	75.7	4.5
640	6	3.6	0.066	124.4	5.3
770	12	4.8	0.086	153.0	5.6
960	4	11.9	0.135	190.8	7.1

As expected the standard deviation (σ) on the measured k_La values increased with increasing stirred speed, due to the higher sensitivity of k_La with the dissolved oxygen concentrations at higher speeds. The spread in these experiments is, however, much less compared to the spread in literature correlations. In Figure 28 a comparison is made with the correlation proposed by van 't Riet (1979), who combined number of measurements of k_La by different methods to obtain:

$$k_La = 2.6 \cdot 10^{-2} \left(\frac{P_g}{V}\right)^{0.4} u_G^{0.5} \tag{26}$$

Linek et al. (1987) critically studied different methods of measurement of oxygen mass transfer coefficients and combined their measurements with experiments from correct methods in the literature to obtain:

$$k_La = 4.95 \cdot 10^{-3} \left(\frac{P_g}{V}\right)^{0.593} u_G^{0.4} \tag{27}$$

To compare the present data with these correlations, the gassed power input was estimated using Equation 19. The results compare good with the equation of Linek et al. (1987) and are higher compared to the work of van 't Riet (1979).

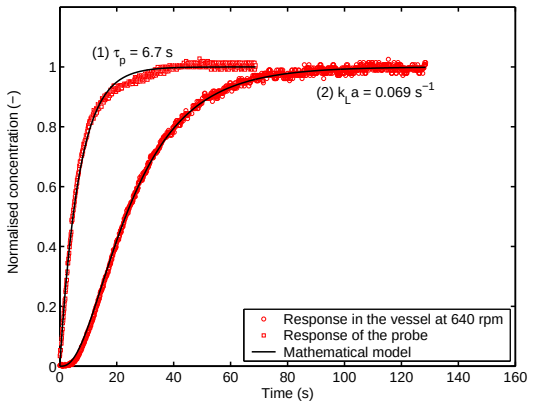

Figure 27: Normalized concentration profiles of the dissolved oxygen probe response compared to the mathematical model.

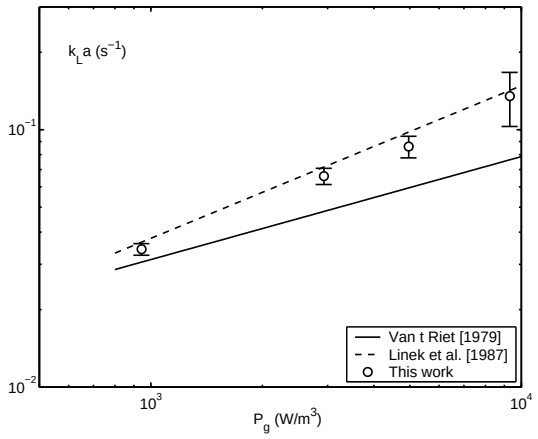

Figure 28: Comparison of the measured volumetric mass transfer coefficient using the dynamic oxygen method with literature correlations. Error bars represent the 95% confidence interval (2 σ)

The mass transfer coefficient, k_L, was calculated from the correlations that were obtained for k_La and a and this resulted in: $k_L \sim (P_g/V)^{0.13}$. When the correlation is based on the individual experiments

the obtained exponent is 0.18. This (small) difference is due to the fact that the k_La was not measured at the lowest stirring speed, which caused a small deviation in the exponent for the interfacial area.

In the literature not much work is performed on the measurement of the mass transfer coefficient in turbulent stirred vessels. The present results correlate very well with the results obtained by Linek et al. (1970), who measured k_La and a in sodium sulfite solutions and obtained: $k_L \approx 2 \cdot 10^{-4}(P_g/V)^{0.14}$. Also the correlation of Yoshida and Miura (1963) is in reasonable agreement with the results in this work. These authors combined measurement of k_La using oxygen absorption with photographic measurement of the bubble diameter and height reading for the measurement of gas hold-up. The obtained exponent in their work was 0.2 (assuming $P \sim N^3$).

7 RESULTS IN NON-COALESCING SYSTEMS

7.1 Profiles of interfacial area and Sauter mean diameter

In Figure 29 the determined values of the measured interfacial area and the calculated Sauter diameter are shown for a system of 0.5 M K_2CO_3 / 0.5 M $KHCO_3$ and air at a superficial velocity of 0.58 cm/s and a stirring speed of 430 rpm. The gas hold-up was only measured using the inclined tube technique, because local measurement using electrical conductivity was not possible due to the high overall conductivity of the medium. A constant gas hold-up throughout the vessel was assumed.

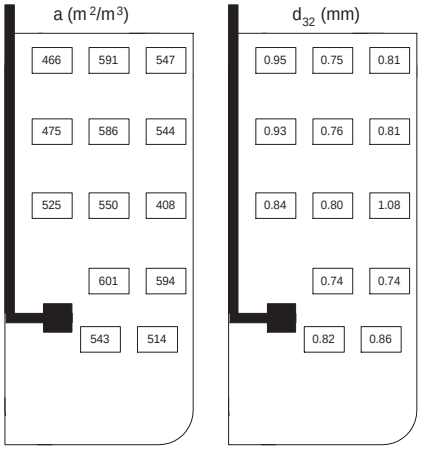

Figure 29: Values of interfacial area and Sauter mean diameter in the buffer solution at a stirring speed of 420 rpm and a superficial gas velocity of 0.58 cm/s.

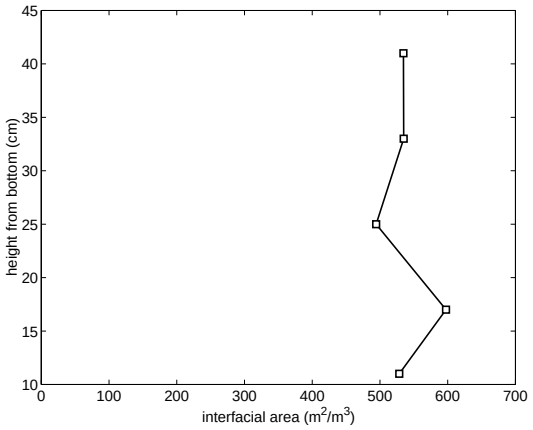

Figure 30: Vertical profile of the gas-liquid interfacial area in the buffer solution at a stirring speed of 420 rpm and a superficial gas velocity of 0.58 cm/s.

In Figure 29 it can be seen that the distribution of the interfacial area is much more homogeneous compared to the coalescing air-water system. This is supported by the vertical distribution of the gas-liquid interfacial area as shown in Figure 30. The interfacial area is approximately constant with height in the vessel. Only just above the impeller plane (17 cm) a small peak in the area is observed. Furthermore, the bubbles are much smaller compared to an air-water system, which was to be expected, as, according to the work of Craig et al. (1993), the electrolyte concentration was high enough for coalescence of bubbles to be suppressed.

7.2 Influence of impeller speed

To show the influence of the speed of the impeller in specific regions in the vessel, two different points are selected; X13, which represents the impeller discharge zone and X7, which represents the bulk of the vessel. The effect of the rotational speed on the interfacial area is shown in Figure 31, which shows that the interfacial area is not a strong function of the position in the vessel in non-coalescing systems. Furthermore,

the existence of a critical impeller speed is demonstrated clearly in Figure 31. A very distinct transition is observed at 250 rpm, below which the interfacial area is almost independent of impeller speed and a region (at higher stirring speeds) where the interfacial area is a strong function of the impeller speed. The critical impeller speed was among others measured by Westerterp et al. (1963) and by Nienow et al. (1977), who found respectively:

$$N_{cr} = \left(\frac{1.22}{D} + \frac{1.25T}{D^2}\right)\left(\frac{\sigma_L g}{\rho}\right)^{0.25} \tag{28}$$

and:

$$N_{cr} = \frac{4\Phi_G^{0.5} T^{0.25}}{D^2} \tag{29}$$

From these relations the following critical impeller speeds could be calculated: 367 rpm from Eq. 28 and 291 rpm from Eq. 29, which are both somewhat higher compared to the observed 250 rpm.

7.3 Influence of superficial gas velocity

In Figure 32 the interfacial area is plotted as a function of the superficial gas velocity at three different stirring speeds (300, 420 and 550 rpm). The interfacial area is a stronger function of the superficial gas velocity at low stirring speeds. At high stirring speeds the area is almost independent of the gas velocity. The obtained results are in good agreement with a correlation of the form: $a \sim u_G^{\beta}$. The obtained exponents were 0.37, 0.17 and 0.01 with increasing impeller speed. Furthermore, the induction of gas when only stirring is applied ($u_G = 0$, i.e. no feed through the sparger) is very high, mainly at high stirring speeds. The decreasing exponent with increasing impeller speed might be caused by an increased gas induction, although the amount of gas induction at gas sparging conditions is, however, unknown.

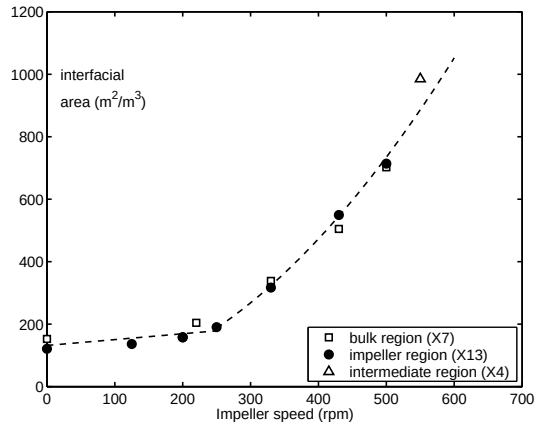

Figure 31: Effect of the impeller speed on the interfacial area in a non-coalescing system at different positions in the vessel

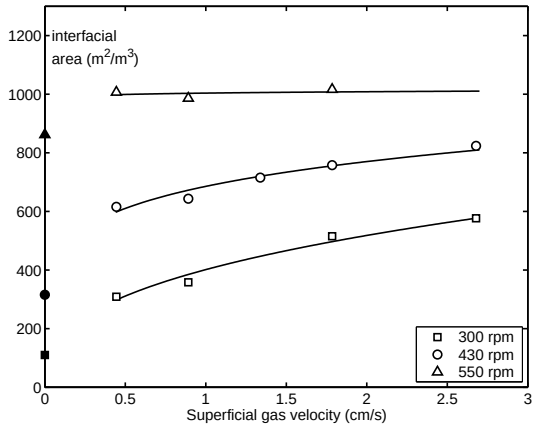

Figure 32: Effect of the superficial gas velocity on the interfacial area in a non-coalescing system at different impeller speeds (position X4). Solid points represent the interfacial area when only stirring is applied.

7.4 Integration to overall values

Due to the homogeneous nature of the non-coalescing systems, mapping of the complete vessels is not necessary. One or two well chosen points in the vessel give a sufficiently accurate value of the interfacial

area. To compare the interfacial area and the Sauter mean diameter with correlations from literature only the data beyond the critical impeller speed were taken into account.

7.5 Interfacial area

In literature no established correlations for the interfacial area, measured using a physical technique, in non-coalescing electrolyte systems are available. The comparison will be performed on the basis of the gas hold-up and the Sauter mean diameter, which are more frequently correlated. The interfacial area beyond the critical impeller speed could be described with: $a = 11.2N^{1.97}$ (dashed line in Figure 31) .

7.6 Gas hold-up

The gas hold-up was determined using the inclined tube method and compared with correlations of Greaves and Barigou (1990) in the different regimes of gas loading as explained in Section 6. Similar to the results for gas hold-up in coalescing systems the data are in good agreement with the correlation for a system with six clinging cavities behind the impeller blades (Eq. 30) as is shown in Figure 33. The equation for 3 large and 3 small cavities (Eq. 31) overestimates the data by approximately 300%, although the experiments at the lower impeller are in this regime according to the criteria of Warmoeskerken and Smith (1985) (assuming that these criteria are also valid for air-electrolyte systems). This equation was therefore not plotted in Figure 33. Greaves and Barigou (1990) found for the regime with 6 clinging cavities in electrolyte systems (regime 1):

$$\varepsilon = 3.86N^{0.92}\Phi_G^{0.41}\left(\frac{D}{T}\right)^{2.56} \tag{30}$$

and for the regime with three alternate cavities (regime 2):

$$\varepsilon = 2.86N^{0.76}\Phi_G^{0.31}\left(\frac{D}{T}\right)^{1.64} \tag{31}$$

In the present study the following relation was obtained: $\varepsilon = 1.29 \cdot 10^{-2}N^{0.87}$. The profile of gas hold-up versus stirring speed does not contain a large change in slope at the critical impeller speed for complete dispersion as was measured in the profile of the interfacial area. This suggests that the obtained discontinuity in this profile was mainly due to a change in bubble diameter.

7.7 Sauter mean diameter

The Sauter mean diameter was compared with the well known equation of Calderbank (1958) for the mean diameter in electrolyte systems:

$$d_{32} = 2.25\left(\frac{\sigma_L^{0.6}}{\left(\frac{P_g}{V}\right)^{0.4}\rho^{0.2}}\right)\varepsilon^{0.4}\left(\frac{\mu_G}{\mu_L}\right)^{0.25} \tag{32}$$

This correlation was determined by the measurement of the interfacial area using a laser scattering technique in a closed system with a known gas fraction. The physical properties and process parameters that are used in the comparison are given in Tables 2 and 3. For fair comparison the gassed power input is estimated by the correlation from Calderbank (1958) (Eq. 15 and 16). The comparison is presented

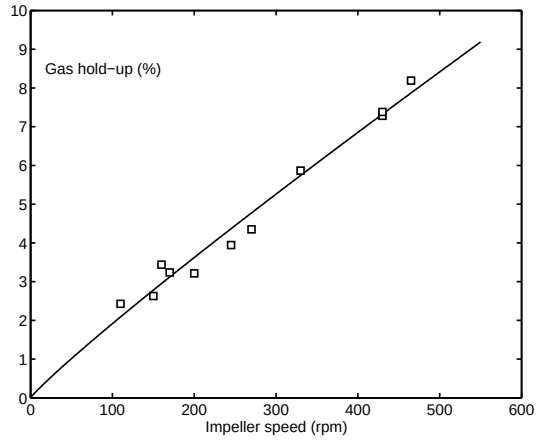

Figure 33: Effect of the impeller speed on the gas hold-up in a non-coalescing system. The solid line is Equation 30.

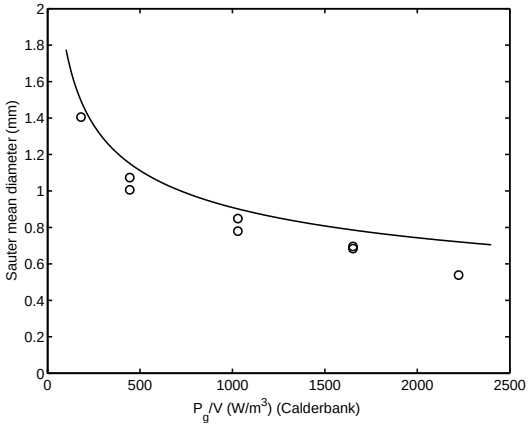

Figure 34: Effect of the impeller speed on the Sauter mean bubble diameter in a non-coalescing system. The solid line is Equation 32.

in Figure 34 and shows that the obtained data in this work are in good agreement with the Calderbank correlation. The obtained diameters were 12% (average relative deviation) lower in this work. The data were also in reasonable agreement with the correlation obtained by Alves et al. (2002), who combined their own measurements with data of Martin (1995) and of Parthasarathy and Ahmed (1994):

$$d_{32} = 0.014 \left(\frac{P_g}{V} \right)^{-0.37} \tag{33}$$

The present data are in good agreement with this correlation, although the average relative deviation is 27%. Although the deviation from the correlation is substantially, it should be noted that also the experimental data on which the correlation was based had a wide spread (a factor 3 at high power inputs). The data obtained in this work can be described (beyond the critical impeller speed) with: $d_{32} = 6.9 \cdot 10^{-3} N^{-1.10}$ and making use of Equation 19: $d_{32} = 0.0115 (P_g/V)^{-0.39}$. The exponent is in close agreement with the correlation of Alves et al. (2002) and also with the theoretically suggested -0.40 (Eq. 17). Contrary to the coalescing air water system (in which the exponent for the Sauter mean diameter in the bulk region was -0.14), coalescence does not seem to play an important role in the air-electrolyte system.

8 RESULTS IN AN AIR-WATER-TOLUENE SYSTEM

In the previous sections measurements were performed in coalescing air-water systems and in non-coalescing air-electrolyte solutions, which were reasonably well investigated in literature. The results were in good agreement with literature correlations and in some parts additional information was obtained. In this section similar techniques will be used to study a system containing air, toluene and water, which is for a large part unexplored.

8.1 Gas hold-up

The gas hold-up was measured using the inclined tube technique in water with toluene fractions of 1, 5, 10 and 20 vol-%. The density difference due to the addition of toluene was maximally 2.6%, which is according to Equation 5 also the maximum error in the gas hold-up, and was therefore neglected. The applied stirring speed was 640 rpm. The results are presented in Figure 35 and show that at low toluene fraction the gas hold-up decreases sharply (more than 30% at 1% toluene). After this initial decrease, the gas hold-up increases to approximately the value for the hold-up in a toluene free system. This value is reached when 20% toluene is

added to the system. This behaviour was also observed by Yoshida et al. (1970), who performed experiments in a 2.57 liter vessel equipped with a 12-vane turbine agitator at two impeller speeds. The gas hold-up was measured in their work by liquid height reading in the vessel. The reason for the initial decrease is not clear. The initial effects were studied separately and the results are reported by Cents et al. (2005).

8.2 Interfacial area

The interfacial area was determined using a similar method compared to the previous sections. The attenuation coefficient was measured at 2 MHz, from which the interfacial area was determined. The results are presented in Figure 36 and show that the interfacial area in the presence of toluene is higher compared to the value in which no toluene is added to the water phase.

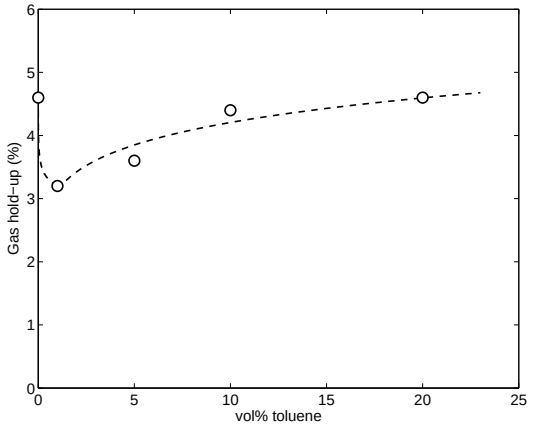

Figure 35: Influence of the toluene volume fraction on the gas hold-up at 640 rpm.

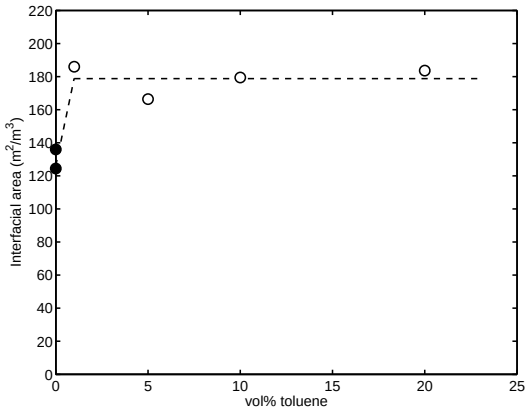

Figure 36: Influence of the toluene volume fraction on the gas-liquid interfacial area at 640 rpm (Position X4).

The trend in the interfacial area with increasing toluene volume fraction is opposite compared to the trend in the gas hold-up. The interfacial area is around 40% higher at 1% toluene compared to pure water, while the gas hold-up is 30% lower. At a volume fraction of 1% toluene several positions in the vessel were measured, and the profile was reasonably homogeneous. This behaviour is unexpected and for this reason further measurements were made on the determination of the size distributions in the presence of toluene compared to the distribution in pure water using attenuation and ultrasonic velocity measurements ranging from 300 kHz to 2.5 MHz. The attenuation coefficient profile is shown in Figure 37. It was not possible to obtain a good fit through the experiments in water containing 1% toluene using a log-normal or normal distribution. The best fit on the experiments at high frequencies using a log-normal distribution is shown as the dotted line in Figure 37. In this case the deviation between the model line and the experiments is very large, mainly at low frequencies. This difference in attenuation coefficient can not be explained by the attenuation caused by the toluene droplets, because this attenuation is mainly in the high frequency regime. In the case of water an accurate fit could be obtained using a log-normal distribution in the attenuation coefficient profile as well as in the ultrasonic velocity profile shown in Figure 38. A good description of the experiments in water with 1% toluene could only be obtained by making use of a bimodal distribution containing at least a certain amount of small (micro) bubbles ($< 200\ \mu$m). The bimodal distribution that was used consisted of two log-normal distributions and a scaling parameter (C_1), which determined the height of both distributions:

$$P(x) = \frac{C_1}{S_1 x\sqrt{2\pi}} \exp\left(-\frac{(\ln(x) - M_1)^2}{2S_1^2}\right) + \frac{(1 - C_1)}{S_2 x\sqrt{2\pi}} \exp\left(-\frac{(\ln(x) - M_2)^2}{2S_2^2}\right) \tag{34}$$

This distribution has five unknown parameters to be determined in the optimization, C_1, M_1, M_2,

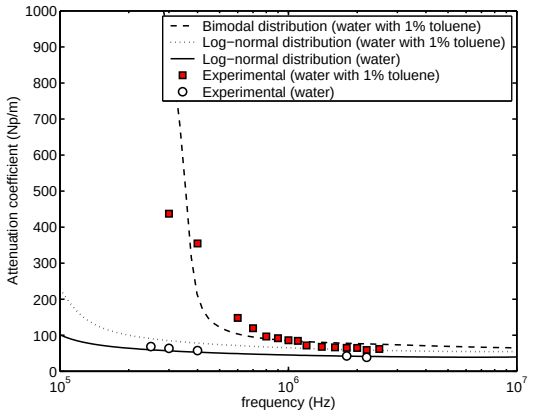

Figure 37: Attenuation coefficient profile of air-water and air-water with 1% toluene with best fit model lines.

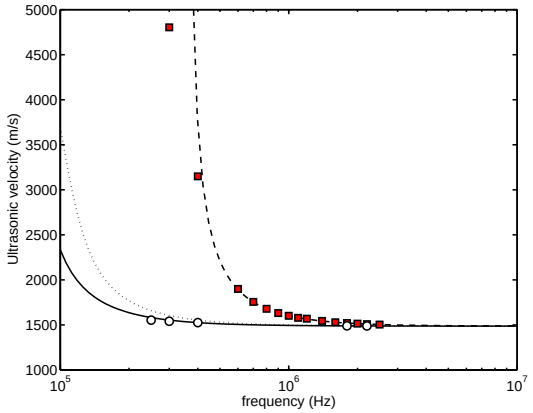

Figure 38: Ultrasonic velocity profile of air-water and air-water with 1% toluene with best fit model lines. For legend see Figure 37.

S_1 and S_2. The assumption $\sigma = 0.1\mu$ was used for both distributions to reduce the number of fit parameters, which was too high compared to the number of experimental data points. Due to the large difference in the ultrasonic velocity and in the attenuation coefficient measurements between low and high frequencies the logarithmic values of the data points were taken into account in the minimization to get a good fit over the complete frequency range. The best fit with this distribution is shown in Figures 37 and 38 and consisted of two bubble classes of 90 μm and 2.6 mm, respectively. The accuracy of the measurements was lower at 300 and 400 kHz, due to the large attenuation coefficient. This caused large disturbances in the signals and complicated the determination of both the attenuation coefficient and the ultrasonic velocity. Mainly for this reason there is some deviation between model and experiments at low frequencies. Further research on the determination of the exact distribution in these systems containing two bubble classes is therefore necessary. The obtained interfacial areas were 94 m^2/m^3 for the small bubbles and 87 m^2/m^3 for the large bubbles. This means that the total interfacial area as determined using the complete profile is in good agreement with the area that is determined when only the attenuation coefficient at 2 MHz is taken into account.

So far, the increase in interfacial area (Figure 36) seems to be due to the presence of micro bubbles in the solution. It remains, however, unclear, whether these micro bubbles participate in the mass transfer process. This will be investigated in the next section.

8.3 Volumetric mass transfer coefficient

The volumetric mass transfer coefficients were measured using the dynamic oxygen method for 1, 5, 10 and 20 vol-% toluene in water. The results (Figure 39) indicate a somewhat similar trend compared to the measured gas hold-up. At small toluene fractions a sharp decrease is observed followed by an increase at higher volume fractions of toluene. The increase in interfacial area at 20% toluene is stronger than the increase of the gas hold-up at the same volume fraction and is almost a factor 2 compared to the interfacial area at 1% toluene in water. The trend was similar as obtained by Yoshida et al. (1970).

A decrease of 21% in k_La at 1% toluene volume fraction is observed, which is in reasonable agreement with the 30% decrease in the gas hold-up. Although an increase in the interfacial area was observed, the decrease in k_La is probably caused by a decrease in the (effective) interfacial area, that was available for mass transfer. The micro bubbles, which were observed, contribute to the measured interfacial area, but do not take part in the mass transfer process. These bubbles might be formed during gas induction from the surface, which was partly supported by measurements of the interfacial area when only stirring was applied (30 m^2/m^3 increase at 1% toluene at position X4). Furthermore, if these small (90 μm) bubbles contain air, they are depleted from oxygen very fast (99% in less than 0.2 s). Their residence time in the solution is probably quite long due to their small rise velocity, while they are only containing nitrogen. This can

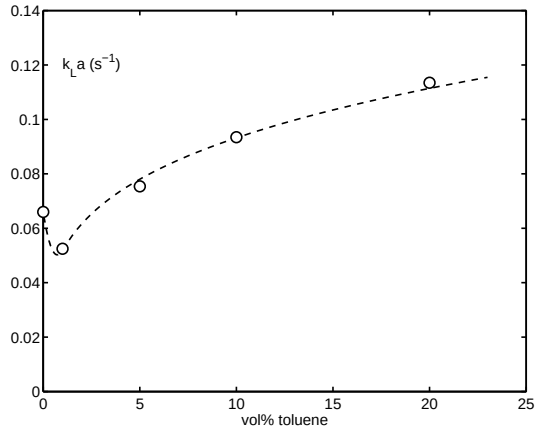

Figure 39: Influence of the toluene volume fraction on the volumetric mass transfer coefficient at 640 rpm.

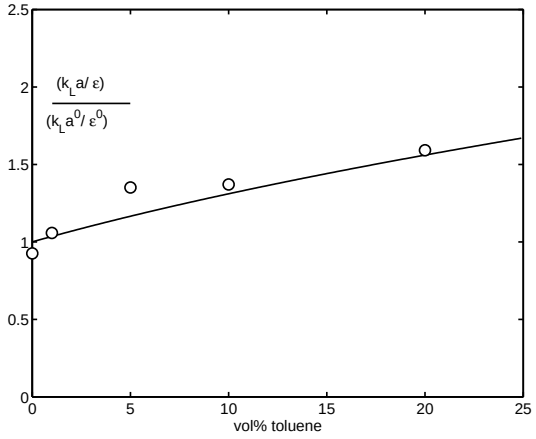

Figure 40: Influence of the toluene volume fraction on $(k_L a/\varepsilon)/(k_L a^0/\varepsilon^0)$ at 640 rpm.

account for an increase in the interfacial area together with a decrease in $k_L a$. The theoretical possibility that the increase in the interfacial was accompanied by a decrease in the mass transfer coefficient, k_L, is not very likely, as this was also not observed in the measurements using the Danckwerts-plot technique (Cents et al., 2001). The decrease in $k_L a$ and in ε at 1% toluene is in good agreement with the decrease in the interfacial area of the large bubbles (30%), which also supports the above considerations.

Although the exact interfacial area that is available for mass transfer is not known accurately, the assumption that the interfacial area is proportional to the overall gas hold-up can be made. In Figure 40 the relative value of the estimated mass transfer coefficient, $(k_L a/\varepsilon)/(k_L a^0/\varepsilon^0)$, is plotted as a function of the toluene volume fraction. The results show a reasonable agreement with a homogenous model of the shuttle mechanism (Bruining et al., 1986; Cents et al., 2001). The enhancement factor due to the presence of a dispersed phase is given by Bruining et al. (1986) in the absence of chemical reaction ($Ha = 0$):

$$\mathrm{E_D} = \sqrt{1 + \varepsilon_D (m_R - 1)} \tag{35}$$

The value for the relative solubility, m_R, was taken from Yoshida et al. (1970) and was 8.2. The value at 5% toluene is somewhat high (15%) compared to the trend, probably due to a somewhat low value for the gas hold-up.

8.4 Droplet diameter

The droplet diameter of toluene was measured at 20% toluene under gassed (G-L-L) and ungassed (L-L) conditions. The attenuation coefficient versus frequency profile is shown in Figure 41. The effect of the gas phase is present in both experiments. In case of the G-L-L system $a_{gas} = 173$ m^2/m^3 and in case of the L-L system $a_{gas} = 40$ m^2/m^3, due to surface aeration. The increasing trend with frequency as shown in Figure 41 can be used to determine the droplet diameter of the liquid phase, while from the increasing attenuation with decreasing frequency, which occurs at the lower frequencies (see Figure 37), the gas phase properties can be determined. The Sauter mean droplet diameter could be determined in both cases and was 164 μm in the G-L-L system and 147 μm in the L-L system. To obtain the droplet size distribution a larger frequency range should be covered. The physical properties of toluene to calculate the model lines were taken from Allegra and Hawley (1972).

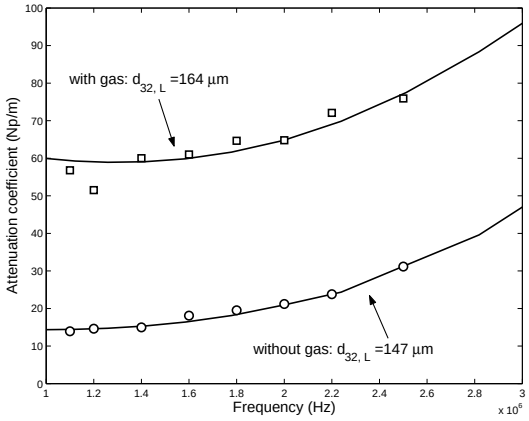

Figure 41: Attenuation coefficient profile of 20% toluene under gassed and ungassed conditions.

9 CONCLUSIONS

In this paper ultrasonic spectroscopy was used for the measurement of the gas-liquid interfacial area in combination with electrical conductivity for the measurement of the gas hold-up. These values were used to calculate the Sauter mean diameter at different positions in the vessel.

The profile that was obtained in the coalescing air-water system, was highly inhomogeneous. The interfacial area was very high in the impeller discharge zone and decreased with increasing height in the reactor. Maximum gas hold-up was obtained at 2/3 of the clear liquid height above the impeller. The bubble diameter increased from small values near the impeller to larger values along with the flow pattern in a stirred vessel. The profile in non-coalescing electrolyte systems was homogeneous. As expected the bubbles were much smaller compared to the coalescing air-water system.

Furthermore, these local values were integrated according to their volumetric space in the reactor to obtain overall values for the mass transfer parameters. The overall gas-liquid interfacial area in the coalescing air-water system could be well described using the established correlation of Calderbank (1958).

The effect of the addition of a small fraction of toluene to a coalescing air-water system is strong. Both the gas hold-up and the volumetric mass transfer coefficient decreased by 20-30%. The gas-liquid interfacial area, however, increased by 40%. It was shown that this was due to the presence of micro bubbles in the solution, which do not take part in the mass transfer process. The enhancing effect due to the addition of larger fractions of toluene could be reasonably well described by a homogeneous model of the shuttle mechanism.

ACKNOWLEDGEMENT

The author wishes to acknowledge D.J.W. Jansen for his contribution to the experimental and theoretical part of this manuscript. B. Knaken is acknowledged for the construction of the set-up.

NOTATION

a	interfacial area, m^2/m^3
c	ultrasonic velocity, m/s
c_G	gas phase concentration, mol/m^3
c_L	liquid phase concentration, mol/m^3
d	measurement distance, m
D	impeller diameter, m
d_{32}	Sauter mean diameter, m
f	volume fraction of a part in the vessel, -
g	gravitational constant, m/s^2
H	liquid height, m
I	signal intensity, V
k_L	liquid phase mass transfer coefficient, m/s
L	length of the liquid in the tube, m
m	ratio of solubility in the liquid phase and in the gas phase, -
M_1, M_2	parameters in log-normal distribution, -
m_R	ratio of the gas solubility in the dispersed and in the continuous phase, -
N	stirring speed, rps
p	pressure, Pa
P, P_g	(gassed) power input, W
S_1, S_2	parameters in log-normal distribution, -
t	time, s
T	vessel diameter, m
u_G	superficial gas velocity, m/s
u_T	terminal rise velocity, m/s
V	volume, m^3
V_{imp}	impeller swept volume = $0.25\pi D^2 W$, m^3
W	impeller blade width, m

Greek

α	attenuation coefficient, Np/m
ε	gas fraction,-
ε_D	dispersed liquid phase fraction,-
μ_G	gas viscosity, Pa s
μ_L	liquid viscosity, Pa s
μ	mean of a size distribution, m
ρ	liquid density, kg/m^3
σ_L	surface tension, N/m
σ	variance of a size distribution, m
τ	residence time, s
Φ	flow rate, m^3/s

Dimensionless numbers

Fl	Gas flow number = $\Phi_G/(N D^3)$
N_P	Power number = $P/(\rho D^5 N^3)$

Sub and Superscript

$0, T, X$	defined in Figure 4
0	value without dispersed phase
abs	absorption
des	desorption
ε	in the dispersion
G	gas phase
i	index for a part in the vessel
it	in the inclined tube
L	liquid phase
P	in the oxygen probe
ves	in the vessel
w	in water

REFERENCES

Allegra, J., Hawley, S., "Attenuation of Sound in Suspensions and Emulsions: Theory and Experiments", J. Acoust. Soc. Am., Vol. 51, 1545–1564 (1972).

Alves, S., Maia, C., Vasconcelos, J., Serralheiro, A., "Bubble Size in Aerated Stirred Tanks", Chem. Eng. J., Vol. 89, 109–117 (2002).

Barigou, M., Greaves, M., "A Capillary Suction Probe for Bubble-Size Measurement", Meas. Sci. Technol., Vol. 2, 318–326 (1991).

Barigou, M., Greaves, M., "Bubble-Size Distributions in a Mechanically Agitated Gas-Liquid Contactor", Chem. Engng Sci., Vol. 47, 2009–2025 (1992).

Barigou, M., Greaves, M., "Gas Hold-up and Interfacial Area Distributions in a Mechanically Agitated Gas-Liquid Contactor", Trans. Instn Chem. Engrs, Vol. 74, 397–405 (1996).

Bouaifi, M., Roustan, M., "Bubble Size and Mass Transfer Coefficients in Dual Impeller Reactors", Can. J. Chem. Eng., Vol. 76, 390–397 (1998).

Bruining, W., Joosten, G., Beenackers, A., Hofman, H., "Enhancement of Gas-Liquid Mass Transfer by a Dispersed Second Liquid Phase", Chem. Engng Sci., Vol. 41, 1873–1877 (1986).

Calderbank, P., "Physical Rate Processes in Industrial Fermentation. Part I: The Interfacial Area in Gas-Liquid Contacting with Mechanical Agitation", Trans. Instn Chem. Engrs, Vol. 36, 443–463 (1958).

Cents, A., Brilman, D., Versteeg, G., "Gas Absorption in an Agitated Gas-Liquid-Liquid System", Chem. Engng Sci., Vol. 56, 1075–1083 (2001).

Cents, A., Brilman, D., Versteeg, G., Wijnstra, P., Regtien, P., "Measuring Bubble, Drop and Particle Sizes in Multiphase Systems with Ultrasound", A.I.Ch.E. J., Vol. 50, 2750–2762 (2004).

Cents, A., Jansen, D., Brilman, D., Versteeg, G., "The Influence of Small Amounts of Additives on Gas Hold-up, Bubble size and Interfacial Area", accepted for Ind. Eng. Chem. Res. (2005).

Cents, A., Kersten, S., Brilman, D., "Gas-Phase RTD Measurement in Gas and Gas-Solids Reactors using Ultrasound", Ind. Eng. Chem. Res., Vol. 42, 5506–5515 (2003).

Craig, V., Ninham, B., Pashley, R., "The Effect of Electrolytes on Bubble Coalescence in Water", J. Phys. Chem., Vol. 97, 10192–10197 (1993).

Dang, N., Karrer, D., Dunn, I., "Oxygen Transfer Coefficients by Dynamic Model Moment Analysis", Biotech. Bioeng., Vol. 19, 853–865 (1977).

Epstein, P., Carhart, R., "The Absorption of Sound in Suspensions and Emulsions.∗ I. Water Fog in Air", J. Acoust. Soc. Am., Vol. 25, 553–565 (1953).

Greaves, M., Barigou, M., "Estimation of Gas Hold-up and Impeller Power in a Stirred Vessel Reactor", Fluid Mixing III, Inst. Chem. Engr., Inst. Chem. Eng. Symp. Series no. 108, 235–255 (1990).

Hughmark, G., "Power Requirements and Interfacial Area in Gas-Liquid Turbine Agitated Systems", Ind. Eng. Chem. Proc. Des. Dev., Vol. 19, 638–641 (1980).

Linek, V., Beneš, P., Vacek, V., Hovorka, F., "Analysis of Differences in k_La Values Determined by Steady State and Dynamic Methods in Stirred Tanks", Chem. Eng. J., Vol. 25, 77–88 (1982).

Linek, V., Mayrhoferová, J., Mošnerová, J., "The Influence of Diffusivity on Liquid Phase Mass Transfer in Solutions of Electrolytes", Chem. Engng Sci., Vol. 25, 1033–1045 (1970).

Linek, V., Vacek, V., Beneš, P., "A Critical Review and Experimental Verification of the Correct Use of the Dynamic Method for the Determination of Oxygen Transfer in Aerated Agitated Vessels to Water, Electrolyte Solutions and Viscous Liquids,", Chem. Eng. J., Vol. 34, 11–34 (1987).

Lu, W.-M., Chi, R.-C., Chien, W.-C., Lin, L.-C., "Measurement of Local Bubble Diameters and Analysis of Gas Dispersion in an Aerated Vessel with Disk Turbine Impeller", J. Chem. Eng. Jap., Vol. 26, 551–557 (1993).

Machon, V., Pacek, A., Nienow, A., "Bubble Sizes in Electrolyte and Alcohol Solutions in a Turbulent Stirred Vessel", Trans. Instn Chem. Engrs, Vol. 75, 339–348 (1997).

Martin, T.1995. Gas Dispersion with Radial and Hydrofoil Impellers in Fluids with Different Coalescence Characteristics. Ph.D. thesis, University of Birmingham.

Mehta, V., Sharma, M., "Mass Transfer in Mechanically Agitated Gas-Liquid Contactors", Chem. Engng Sci., Vol. 26, 461–479 (1971).

Meng, A., Hill, G., Dalai, A., "Modified Volume Expansion Method for Measuring Gas Hold-up", Can. J. Chem. Eng., Vol. 80, 194–199 (2002).

Nelder, J. A., Mead, R., "A Simplex Method for Function Minimization", Computer Journal, Vol. 7, 308–313 (1965).

Nienow, A., Wisdom, D., Middleton, J., "Effect of Scale and Geometry on Flooding, Recirculation and Power in Gassed Stirred Vessels", Proc. 2^{nd} Euro. Conference on Mixing, Cambridge UK, F1, 1–16 (1977).

Pacek, A., Moore, I., Nienow, A., Calabrese, R., "Video Technique for Measuring Dynamics of Liquid-Liquid Dispersion During Phase Inversion", A.I.Ch.E. J., Vol. 40, 1940–1949 (1994).

Parthasarathy, R., Ahmed, N., "Sauter Mean and Maximum Bubble Diameters in Aerated Stirred Vessels", Trans. Instn Chem. Engrs, Vol. 72, 565–572 (1994).

Riet, K. v. t., "Review of Measuring Methods and Results in Non-Viscous Gas-Liquid Mass Transfer in Stirred Vessels", Ind. Eng. Chem. Proc. Des. Dev., Vol. 18, 357–364 (1979).

Rols, J., Condoret, J., Fonade, C., Goma, G., "Mechanism of Enhanced Oxygen Transfer in Fermentation using Emulsified Oxygen-Vectors", Biotech. Bioeng., Vol. 35, 427–435 (1990).

Wachsen, O., Himmler, K., Cornils, B., "Aqueous Biphasic Catalysis: Where the Reaction Takes Place", Catalysis Today, Vol. 42, 373–379 (1998).

Warmoeskerken, M., Smith, J., "Flooding of Disk Turbines in Gas-Liquid Dispersions: a new Description of the Phenomenon", Chem. Engng Sci., Vol. 40, 2063–2071 (1985).

Westerterp, K., van Dierendonck, L., de Kraa, J., "Interfacial Areas in Gas-Liquid Contactors", Chem. Engng Sci., Vol. 18, 157–176 (1963).

Yoshida, F., Miura, Y., "Gas Absorption in Agitated Gas-Liquid Contactors", Ind. Eng. Chem. Proc. Des. Dev., Vol. 2, 263–268 (1963).

Yoshida, F., Yamane, T., Miyamoto, Y., "Oxygen Absorption into Oil-in-Water Emulsions", Ind. Eng. Chem. Proc. Des. Dev., Vol. 9, 570–577 (1970).